Author/s:
Anderson, AJ;Crameri, JJ;Ang, C-S;Malcolm, TR;Kang, Y;Baker, MJ;Palmer, CS;Sharpe, AJ;Formosa, LE;Ganio, K;Baker, MJ;McDevitt, CA;Ryan, MT;Maher, MJ;Stojanovski, D

Title:
Human Tim8a, Tim8b and Tim13 are auxiliary assembly factors of mature Complex IV

Date:
2023-06-05

Citation:
Anderson, A. J., Crameri, J. J., Ang, C. -S., Malcolm, T. R., Kang, Y., Baker, M. J., Palmer, C. S., Sharpe, A. J., Formosa, L. E., Ganio, K., Baker, M. J., McDevitt, C. A., Ryan, M. T., Maher, M. J. & Stojanovski, D. (2023). Human Tim8a, Tim8b and Tim13 are auxiliary assembly factors of mature Complex IV. EMBO Reports, 24 (8), https://doi.org/10.15252/embr.202256430.

Persistent Link:
https://hdl.handle.net/11343/333647

Human Tim8a, Tim8b and Tim13 maintain late-stage Complex IV assembly

Alexander J. Anderson [1,2], Jordan J. Crameri [1,2], Ching-Seng Ang [2], Tess R. Malcolm [2,3], Yilin Kang [1,2], Megan J. Baker [1,2], Catherine S. Palmer [1,2], Alice J. Sharpe [4], Luke E. Formosa [4], Katherine Ganio [5], Michael J. Baker [1,2], Christopher A. McDevitt [5], Michael T. Ryan [4], Megan J. Maher [2,3,6] and Diana Stojanovski [1,2,#]

[1] Department of Biochemistry and Pharmacology, The University of Melbourne, Parkville, 3052, Victoria, Australia

[2] The Bio21 Molecular Science and Biotechnology Institute, The University of Melbourne, Parkville, 3052, Victoria, Australia

[3] School of Chemistry, The University of Melbourne, Parkville, 3052, Victoria, Australia

[4] Department of Biochemistry and Molecular Biology, Monash Biomedicine Discovery Institute, Monash University, Clayton, 3168, Victoria, Australia

[5] Department of Microbiology and Immunology, The Peter Doherty Institute for Infection and Immunity, The University of Melbourne, Parkville, 3052, Victoria, Australia

[6] Department of Biochemistry and Genetics, La Trobe Institute for Molecular Science, La Trobe University, Bundoora, 3086, Victoria, Australia

Corresponding Author: **Diana Stojanovski**

E-mail: d.stojanovski@unimelb.edu.au

Running Title: Human small TIMs in Complex IV assembly

Total Character Count: 68,652

Abstract (175 words)

Human Tim8a and Tim8b are paralogous intermembrane space proteins of the small TIM chaperone family. Yeast small TIMs function in the trafficking of proteins to the outer and inner mitochondrial membranes. This putative import function for hTim8a and hTim8b has been challenged in human models, but their precise molecular function(s) remains undefined. Likewise, the necessity for human cells to encode two Tim8 proteins and whether any potential redundancy exists is unclear. We demonstrate that hTim8a and hTim8b function in the assembly of cytochrome *c* oxidase (Complex IV). Using affinity enrichment mass spectrometry, we define the interaction network of hTim8a, hTim8b and hTim13, identifying subunits and assembly factors of the Complex IV COX2 module. hTim8-deficient cells have a COX2 and COX3 module defect and exhibit an accumulation of the Complex IV S2 subcomplex. These data suggest that hTim8a and hTim8b function in assembly of Complex IV via interactions with intermediate-assembly subcomplexes. We propose that hTim8-hTim13 complexes are auxiliary assembly factors involved in the formation of the Complex IV S3 subcomplex during assembly of mature Complex IV.

Key words: Complex IV/mitochondria/protein assembly/protein trafficking/small TIMs

Introduction

The yeast small TIM family of chaperones (Tim8, Tim9, Tim10, Tim12 and Tim13) function in the mitochondrial intermembrane space (IMS) to shield unfolded, hydrophobic membrane proteins and maintain an import-competent state for downstream translocation [1, 2]. Yeast Tim9-Tim10 hexameric complex ($Tim9_3$-$Tim10_3$) facilitates the transport of metabolite carrier proteins to the inner membrane [3], whereas the $Tim8_3$-$Tim13_3$ complex [4] preferences β-barrel cargo directed to the outer membrane [5]. Subsequent work highlighted an overlap of substrates [6], and showed that Tim8 and Tim13 are non-essential for yeast viability [7]. The small TIM proteins are unstable as monomeric units and acquire stability in their heterooligomeric hexameric forms (~70 kDa), which are the functional chaperone entities in yeast [8].

Human cells have six small TIM proteins; hTim8a, hTim8b, hTim9, hTim10a, hTim10b, and hTim13 [9]. The human $Tim9_3$-$Tim10a_3$ hexamer delivers membrane proteins to the TIM22 translocase, where the $Tim9_2$-$Tim10a_3$-$Tim10b_1$ hexamer aids their translocation. Human Tim8a and Tim8b are paralogues, which arose through gene duplication with the evolution of chordate animals and diverged as more differentiated body plans emerged [10]. hTim8a and hTim8b share 49% sequence identity and show most divergence in the putative substrate binding regions at both the N- and C-termini. Human Tim8b has broad tissue expression, most prominently in endocrine and skeletal muscle tissue [9], while hTim8a is predominantly expressed in the liver and brain, and has particularly high levels of expression in the fetal brain [11, 12]. Mutations in *TIMM8A* are associated with the degenerative neuronopathy Mohr-Tranebjærg syndrome (MTS) [13]. In contrast, there is currently no disease association with *TIMM8B*, which may imply a unique and/or non-essential function. Studies using yeast mitochondria expressing hTim8a [14] proposed the loss of hTim8a-mediated import of Tim23 as the pathomechanism underlying MTS. More recently, *TIMM8A* gene-edited human cell models of MTS showed that loss of hTim8a does not perturb Tim23 import, but rather results in Complex IV (cytochrome *c* oxidase) dysfunction giving rise to increased levels of reactive oxygen species (ROS) and sensitises neurons to apoptotic induction [15].

Despite this insight into the mechanisms of mitochondrial dysfunction in MTS, the molecular basis of Complex IV deficiency in cells lacking hTim8a is unclear. It remains unknown if hTim8b also plays a role in Complex IV biology. In the canonical model of Complex IV assembly, mature Complex IV is assembled from modules built around core subunits that are encoded by the mitochondrial DNA (MT-CO1, MT-CO2 and MT-CO3) [16]. During the assembly process these modules come together to form assembly intermediates known as subcomplexes or subassemblies (**Fig EV1A)**. MT-CO1 (COX1 module/*S1 subcomplex*) combines with the *scaffold* of COX4I1–COX5A to form the *S2 subcomplex*. Independently, MT-CO2 assembles with associated subunits (COX5B, COX6C, COX7B, COX7C, COX8A) to create the COX2 module and is integrated with the S2 subcomplex to form the *S3 subcomplex*. MT-CO3 and COX6A, COX6B, COX7A, NDUFA4, also known as the COX3 module, are added to the S3 subcomplex to give rise to mature Complex IV (*S4 mature and monomeric assembly*) [16, 17]. The sequence of assembly continues to be refined and the independence of the core modules has been challenged [18-20]. What is clear is that the formation and biogenesis of Complex IV relies on numerous assembly factors (>30), that facilitate the integration of co-factors and combining of subcomplexes to build mature Complex IV [21].

We interrogated the organisation of the human Tim8 proteins and mapped their interactions to explore the molecular function of these proteins in Complex IV biogenesis. Here, we show that hTim8a and hTim8b largely share the same protein interaction network across cell types but are unable to completely rescue the loss of the other paralogue. We show function of hTim8a and hTim8b in Complex IV assembly, specifically an interaction with COX2 module assembly factors and subunits of the Complex IV S3 subcomplex. Loss of hTim8 proteins renders subunits of the COX2 and COX3 modules more easily extracted from the membrane and causes stalling at the S2 subcomplex (MT-CO1–COX4I1–COX5A), as observed in other cases of dysfunctional COX2 module and COX3 module assembly [22, 23]. We propose that hTim8a, hTim8b and hTim13 function as auxiliary chaperones/assembly factors in the formation of the S3 subcomplex of Complex IV.

Results

The interaction network of hTim8a, hTim8b and hTim13 is similar across cell types

The interaction profiles of hTim8a and hTim8b in mitochondria were investigated using affinity enrichment mass spectrometry. hTim8a^{FLAG} and hTim8b^{FLAG} (C-terminal tags) were expressed in respective CRISPR/Cas9 gene-edited (knock-out; KO) cell lines in HEK293 or SH-SY5Y backgrounds. For clarity, these cell models are referred to as: hTim8a$^{KO\ HEK}$ (*TIMM8A* KO in HEK293); hTim8a$^{MUT\ SH}$ (*TIMM8A* mutant in SH-SY5Y cells – a heterozygous mutant with one wild-type allele but no hTim8a protein); hTim8b$^{KO\ HEK}$ (*TIMM8B* KO in HEK293) and hTim8b$^{KO\ SH}$ (*TIMM8B* KO in SH-SY5Y cells). Creation of the cell lines is described in detail [15], and they were generated to reflect the distinct tissue expression profiles of hTim8a and hTim8b. hTim8a^{FLAG} and hTim8b^{FLAG} expressed in the respective knock-out cells are functional based on the restoration of AIFM1 and COX17 levels in hTim8a$^{KO\ HEK}$ cells relative to the control (**Fig 1A**); and recovery of COX17, COX6A1 and MT-CO2 in hTim8b$^{KO\ HEK}$ cells (**Fig 1B**).

Immunoprecipitation of hTim8b^{FLAG} under native conditions from HEK293 cells strongly enriched hTim8a and hTim13 indicating stable interactions between these proteins, but weak interactions with other proteins (**Fig EV1B**; **Dataset EV1**). Dithiobis-succinimidyl propionate (DSP) crosslinking and affinity enrichment mass spectrometry in mitochondria isolated from HEK293 cells expressing hTim8a^{FLAG} (**Fig 1C**) or hTim8b^{FLAG} (**Fig 1D**); or SH-SY5Y cells expressing hTim8a^{FLAG} (**Fig 1E**) or hTim8b^{FLAG} (**Fig 1F**) showed similar interaction networks for both hTim8a and hTim8b across both cell types. This included: (i) substrates of the Mitochondrial Intermembrane Space Assembly (MIA) import machinery, which oxidises incoming cysteine-rich IMS proteins; and (ii) Complex IV assembly factors and subunit, including COA4, COA6, COA7 and COX6B1, which were common across all four datasets (**Fig 1C-F**; **Dataset EV1**). Enriched in at least two of the four cell lines were Complex IV assembly factors CMC1, COA5, COX19, SCO1 and SCO2, electron carrier cytochrome *c* (CYCS), plus the subunits COX4I1, COX5A and COX6C (**Dataset EV1**). These Complex IV subunits and assembly factors are members of the S3 subcomplex comprised by the COX1 module, COX2 module and the COX4I1–COX5A scaffold [21]. Crosslinking and

immunoprecipitation of hTim8b^{FLAG} from HEK293 and hTim8a^{FLAG} from SH-SY5Y cells yielded the most Complex IV protein interactors (19 and 15 significantly enriched, respectively) (**Fig 1D-E**; **Dataset EV1**), correlating with the tissue expression profiles of the paralogues. There were no unique interactors of either hTim8a or hTim8b across the cell lines used. Lower protein expression of hTim8b^{FLAG} retained key interactors COA4, COA6, COA7, CMC1, COX6B1, COX6C and CHCHD-family proteins in HEK293 cells (**Fig EV1C**; **Dataset EV1**), and interactions with COA4, COA6 and COA7 were maintained SH-SY5Y cells (**Fig EV1D**; **Dataset EV1**). hTim13^{FLAG} expressed in HEK293 cells showed the same interaction network, which included 9 Complex IV proteins also identified as hTim8a^{FLAG} and hTim8b^{FLAG} interactors (**Fig 1G**; **Dataset EV1**). Both hTim8a and hTim8b were strongly enriched by hTim13^{FLAG}. Across the five datasets (**Fig 1C-G**), a total of 147 proteins were enriched, of which 72 proteins were common to hTim8a^{FLAG}, hTim8b^{FLAG} and hTim13^{FLAG} (enriched ≥4-fold in ≥3 / 5 immunoprecipitations). 85% of the common interactors localise to the IMS or inner membrane (**Fig 1H**) aligning with the IMS localisation of small TIM proteins. By comparison, crosslinking and immunoprecipitation of hTim10b^{3xFLAG} from HEK293 mitochondria enriched known interacting partners of the TIM22 complex hTim9, hTim10a and Tim29 [24] (**Fig EV1E**), and captured components of the MIA machinery and MIA substrates such as hTim8a, hTim8b, hTim13, COA7 and COX6B1. However, numerous Complex IV subunits and assembly factors were not readily apparent.

STRING analysis [25] clustered the 72 common interactors of hTim8a, hTim8b and hTim13 into groups, including: the electron transport chain (predominantly Complex I and IV); MICOS/MIB complex, which is maintains mitochondrial architecture; mitochondrial translocase subunits (TIMM and TOMM), or Mia40 (CHCHD4) substrates (**Fig 2A**). To interrogate the functional interplay of these interactions we cross-referenced if the identified interactors had changes in their protein abundance from mitochondrial proteomics data of the respective knock-out cell lines [15] (**Fig 2B-C**). In Fig **2B** and **2C** each quadrant indicates a ±1.5-fold change in steady-state protein level in the absence of hTim8a or hTim8b in HEK293 (**Fig 2B**) or SH-SY5Y cells (**Fig 2C**). HEK293 mitochondria lacking either hTim8a or hTim8b

showed depletion of hTim13 in addition to Complex IV assembly factors and MIA substrates COX17 and COA4 (**Fig 2B**), while the hTim8b^{FLAG} interactors CMC4, COA7, CHCHD5, CHCHD7, and CCDC58 are depleted in hTim8b$^{KO\ HEK}$ mitochondria alone (**Fig 2B**). In SH-SY5Y cells, hTim13, MT-CO2 and COX6B1 are depleted in both hTim8a- and hTim8b-deficient mitochondria. This implies the function(s) of hTim8a and hTim8b is required, directly or indirectly, for the persistence of these proteins and suggests the Complex IV related interactors of hTim8a and hTim8b are functionally relevant.

Exploring the functional implications of the small TIM interaction network

Mia40 (CHCHD4) substrates [26], represented one third of the hTim8a, hTim8b and hTim13 common interacting network. Compared to other respiratory complexes, a disproportionate number of Complex IV assembly factors and subunits are Mia40 substrates (Complex IV has 10:14 cys-rich assembly/subunits : total subunits, Complex I has 4:45, Complex III 1:11) [27]. This includes COX17, COA4, COA6, COA7 and COX6B1, which show decreased abundance in hTim8a or hTim8b-deficient cells [15]. Crosslinked immunoprecipitation of Mia40^{FLAG} expressed in HEK293 cells enriched hTim8a, hTim8b and hTim13, but not the other small TIM family members and known MIA substrates hTim10a, hTim10b and hTim9 (**Fig EV2A**; **Dataset EV1**), suggesting that interaction between hTim8a, hTim8b, hTim13 and Mia40 may have functional significance. The Mia40^{FLAG} interaction profile was concordant with previous affinity enrichment analyses of Mia40 interactors [28, 29]. Notably, COA4, COA6, and COX6B1 were among the most strongly enriched known MIA substrates.

We assessed if hTim8a or hTim8b were acting pre- or post MIA in the import of substrates, in particular Complex IV assembly factors and subunits, to facilitate the biogenesis of these proteins. Import of the control [^{35}S]-Tim23 and test MIA substrates [^{35}S]-hTim10a, [^{35}S]-COX6B1, [^{35}S]-COX17, [^{35}S]-COA6 into mitochondria from control and hTim8b$^{KO\ HEK}$ cells suggested no import defect in cells lacking hTim8b (**Fig EV2B-F**). As MIA import defects are associated with cytosolic accumulation of IMS proteins [30], we examined the levels of known

MIA substrates [26] in total, mitochondrial and cytosolic fractions of control and hTim8b$^{KO\ HEK}$ cells following treatment with the proteasome inhibitor MG132 (**Fig EV2G**; **Dataset EV2**). Increase in the cytosolic levels of UQCRH (Complex III) in both cell lines, a substrate degraded by the proteasome [31], showed the validity of the approach. However, MIA substrates were unaffected, suggesting hTim8b is not acting at a pre-MIA stage in the biogenesis of cysteine-rich IMS proteins. Studies in both yeast and human cells indicate many MIA substrates are degraded by *i*-AAA protease Yme1L [32, 33]. We considered if hTim8b functions to protect IMS proteins from intramitochondrial degradation post-import as Yme1L was enriched in all five small TIM immunoprecipitations (**Fig 1C-G**). *YME1L*-targeted siRNA treatment (**Fig EV2H**) failed to recover hTim8b^{FLAG} interactors and MIA substrates such as COX17 (**Fig EV2I**), while Yme1L substrates such as OCIAD2, STARD7, SLMO2, MICU1 and TIM23 showed increased abundance independent of cell line background (**Fig EV2I**; **Dataset EV2**). These data confirmed that hTim8b does not play a direct role in the import or Yme1L-mediated proteostasis of MIA substrates and thus we explored the function of hTim8a and hTim8b in Complex IV biogenesis.

Loss of hTim8a or hTim8b influences Complex IV COX2 and COX3 module subunits and assembly factors

Complex IV subunits and assembly factors were decreased in abundance across quantitative mitochondrial proteomics datasets from cells lacking hTim8a or hTim8b [15]. We interrogated these datasets to identify any trends for further investigation (**Fig 3A**). Particularly impacted were COX2 module assembly factors (COX17, COA6, COA7 and SCO2) and subunits (MT-CO2, COX5B, COX6C, COX7C and COX8A). Furthermore, subunits of the COX3 module (MT-CO3, COX6A1, COX6B1, COX7A1 and NDUFA4), which is formed after COX2 assembly, are reduced in abundance in addition to the MT-CO3 assembly factor HIGD2A [23] (**Fig 3A**; **Fig EV3A**, SH-SY5Y proteomics data mapped to Complex IV structure PDB5Z62 [34]). Consistent with perturbations to Complex IV, hTim8a$^{KO\ HEK}$ and hTim8b$^{KO\ HEK}$ cells show an increase in reactive oxygen species (ROS) or a sensitivity to ROS induction (**Fig EV3B**). The

most striking feature common to all hTim8-deficient cell lines was the decreased abundance of the assembly factor and copper chaperone COX17 (**Fig 3A**), thought to be responsible for Cu(I) delivery to the COX1 and COX2 modules [35, 36].

To ascertain if the changes we observe to Complex IV subunits and assembly factors in cells lacking hTim8a or hTim8b is a secondary impact of COX17 depletion, we targeted *COX17* using CRISPR/Cas9 in HEK293 and SH-SY5Y cells ($COX17^{MUT\ HEK}$ – a mutant protein product is translated, but no wild-type COX17 present; $COX17^{KO\ SH;}$ *COX17* KO in SH-SY5Y) (**Fig EV3C**). Quantitative mitochondrial proteomics showed depletion of numerous Complex IV subunits of the COX2 and COX3 modules upon loss of COX17 (**Fig 3B-C**, **Fig EV3D**; **Dataset EV3**). This phenotype was more severe than that observed in cells lacking hTim8a and hTim8b (**Fig 3A**). Loss of COX17 did not affect other assembly factors of the COX2 and COX3 modules such as COA4, COA6, COA7 and HIGD2A (**Fig 3B-C**), which are altered in hTim8a and hTim8b-deficient cells. MT-CO1 and assembly factors of the COX1 module (COA3, COA5, COX15, SMIM20, SURF1) were unaffected or increased in abundance in the absence of COX17 (**Fig 3B-C**; **Dataset EV3**). HEK293 cells lacking COX17 show increased levels of hTim8a, hTim8b and hTim13 (**Fig 3B**), concomitant with an increase in the endogenous hTim8a-containing complex observed by BN-PAGE (**Fig 3D**). Published datasets show hTim8a, hTim8b and hTim13 abundance increases in other models of COX2 and COX3 mis-assembly [23, 37]. Much like COX17 and hTim8-deficient cells, mitochondria lacking the assembly factors COA6 and HIGD2A are depleted of COX2 and COX3 module subunits such as COX6A1, COX6B1, COX7A2 and NDUFA4, plus have higher levels of hTim8a, hTim8b and hTim13 (**Table 1-2**). The loss of mature Complex IV was observed in SH-SY5Y lacking COX17 and the accumulation of an intermediate subcomplex (labelled *) was present in both COX17-deficient cell lines (**Fig 3D**). Crosslinked affinity enrichment of ^{FLAG}COX17 (N-terminal tag) from $COX17^{MUT\ HEK}$ mitochondria confirmed that COX17 interacts with hTim8a, hTim8b, and hTim13 (**Fig 3E**). Given, the role of COX17 in copper handing we assessed copper levels in $hTim8b^{KO\ HEK}$ mitochondria using inductively coupled plasma-mass spectrometry (ICP-MS). Unlike mutant SCO1 and SCO2 cells in which copper delivery to MT-CO2 (directly

downstream of COX17) is perturbed [38], we observed that copper levels in mitochondria lacking hTim8b did not substantially change (**Fig 3F**; **Dataset EV4**). Further, neither recombinant hTim8a nor hTim8b were able to bind copper, compared to the known copper-binding assembly factor COA6 [39] (**Fig 3G**). Given the comparative severity of Complex IV deficiency between COX17 and hTim8a or hTim8b knock-out cells, and unperturbed copper regulation in mitochondria lacking hTim8b, it is unlikely hTim8a or hTim8b function directly with COX17 in the metalation of MT-CO2. However, the similar loss of mature Complex IV assembly and COX2 and COX3 module subunits suggests the small TIMs act in an adjacent stage of Complex IV biogenesis.

We set out to characterise the stage of Complex IV biogenesis mediated by hTim8a and hTim8b by first examining the independent assembly of the COX2 module. The biogenesis of mitochondrial DNA (mtDNA) encoded subunits was assessed with a 2 h 'pulse' of [^{35}S]-Met in control and hTim8-deficient HEK293 cells, followed by removal of the radiolabel and chase of mtDNA-encoded subunits for 3 and 24 hours. Analysis using SDS-PAGE suggested the hTim8 proteins are not involved in the translation or stability of any mtDNA encoded subunits of Complex IV (**Fig 4A**). The *in vitro* import and assembly of nuclear encoded subunits of the COX2 module showed no difference in the assembly profile of [^{35}S]-COX6C and [^{35}S]-COX7C by BN-PAGE in mitochondria isolated from control or hTim8a$^{MUT\ SH}$ and hTim8b$^{KO\ HEK}$ cells (**Fig 4B-C**). These results provide evidence that the independent assembly of the COX2 module does not involve hTim8a or hTim8b. Therefore, the cause of the COX2 and COX3 module deficiency observed in hTim8-deficient cells (**Fig 3A**) may lie in a subsequent stage of assembly.

To pinpoint where in the Complex IV assembly pathway the hTim8 proteins act, we investigated how the pool of Complex IV assembly intermediates changes in the absence of either paralogue. This was achieved using the scaffold subunit COX4I1 as bait to enrich Complex IV intermediate subcomplexes from mitochondria; as the COX4I1 scaffold is present in each subcomplex during the assembly to mature Complex IV [21] (**Fig EV1A**). COX4I1^{FLAG} was introduced into control, COX17$^{MUT\ HEK}$, hTim8b$^{KO\ HEK}$ and hTim8a$^{MUT\ SH}$ cells by viral

transduction. Affinity enrichment mass spectrometry showed that in the absence of COX17 the association of COX4I1^{FLAG} with MT-CO1 and COX1 module assembly factors CMC1, COX11, COX19 and SURF1 was increased, indicating an accumulation of the early-stage S2 subcomplex (COX4I1–COX5A–MT-CO1) in the absence of COX17 (**Fig 4D**; **Dataset EV1**). Consistent with a COX2 module defect and loss of the S3 subcomplex (COX4I1–COX5A–MT-CO1–COX2 module), COX4I1^{FLAG} interactions with MT-CO2, COX7B, COA6, COX6B1 and NDUFA4 were decreased or lost in COX17$^{MUT\ HEK}$ compared to control mitochondria. In the absence of hTim8b, the interaction of COX4I1^{FLAG} with COX2 subunits was maintained, implying the COX2 module is sufficiently assembled to engage with the S2 subcomplex (**Fig 4D**). Yet COX4I1^{FLAG} also enriched COX2 assembly factors TMEM177, COX20 and SCO1 which function together in the biogenesis of MT-CO2 [40], suggesting the enrichment of predominantly nascent COX2 module. As in COX17$^{MUT\ HEK}$ mitochondria, the COX1 assembly factors COX11, COX15, COX19 and SURF1 were more robustly enriched with COX4I1 from hTim8b$^{KO\ HEK}$; SURF1 being required for progression from S2 to S3 subcomplex [41, 42] (**Fig 4D**). Similarly, COX4I1^{FLAG} interaction with assembly factors COX15, COX19, SURF1, and SCO1 was more enriched in the hTim8a$^{MUT\ SH}$ background. In the absence of hTim8a, COX4I1^{FLAG} enriched COX2 module subunits except for COX6C, suggesting some overlap of COX2 assembly and the transition from S2 to S3 subcomplex (**Fig 4D**). Subunits of respiratory complexes I and III were highly enriched from each knock-out (**Dataset EV1**), consistent with Complex IV biogenesis within respiratory supercomplexes being favoured when its monomeric assembly is compromised [43, 44]. Collectively, the results suggest hTim8 proteins contribute to the progression of the S2 subcomplex into the S3 subcomplex.

Sodium carbonate treatment of isolated mitochondria revealed membrane subunits of COX2 and COX3 modules (COX5B, COX6C, MT-CO3, COX6A1, COX7A2, COX7A2L) are more easily extracted from the membrane in HEK293 cells lacking hTim8a or hTim8b, implying a lack of incorporation into stable monomeric Complex IV (**Fig 4E**; **Dataset EV5**). Immunoblotting of mitochondria isolated from hTim8a$^{MUT\ SH}$ or hTim8b$^{KO\ HEK}$ cells with COX4I1 antibody confirms accumulation of a subcomplex (**Fig 4F**, labelled *****) relative to the levels of

277 the mature Complex IV (intensity of subcomplex as % of mature Complex IV). Compared to
278 their relevant control mitochondria, the subcomplex increased ~4.5-fold in Tim8a^{MUT} SH-SY5Y
279 mitochondria and ~1.8-fold in hTim8b$^{KO\ HEK}$ mitochondria. By BN-PAGE and immunoblotting
280 with antibodies against MT-CO1, MT-CO2 and COX4I1 we can conclude that the subcomplex
281 is increased in COX17$^{MUT\ HEK}$, hTim8a$^{KO\ HEK}$ and hTim8b$^{KO\ HEK}$ cells, and lacks MT-CO2 but
282 contains MT-CO1 and COX4I1 (**Fig 4G**). Thus, we infer that this accumulating subcomplex is
283 the S2 subcomplex, the assembly intermediate prior to incorporation of the COX2 module into
284 the S3 subcomplex.

285

286 **hTim8a and hTim8b support formation of the Complex IV S3 subcomplex**

287 To validate the function of the hTim8 proteins in the formation of the S3 subcomplex we
288 performed complexome analysis. Mitochondria from SILAC-labelled control and hTim8-
289 deficient HEK293 and SH-SY5Y cells were separated by BN-PAGE and analysed by mass
290 spectrometry (**Dataset EV5)**. The subcomplex previously identified by immunoblot (**Fig 4F-G**)
291 was consistent with the COX4I1–COX5A–MT-CO1 S2 subcomplex (white dashed box, ~210
292 kDa,), which was found to also migrate with COX1 module assembly factors CMC1, COA3,
293 SMIM20 and SURF1 in HEK293 cells (**Fig 5A**). The COX2 module subunits COX7C, COX5B
294 and COX7B were also detected in this region, but the core MT-CO2 and other COX2 module
295 components were absent (**Fig 5A**). Relative to control mitochondria, hTim8b$^{KO\ HEK}$ had
296 elevated levels of COX4I1, COX5A, MT-CO1 and SURF1 in this region (**Fig 5A**, right panel).
297 Although still the dominant arrangement, all Complex IV subunits were less abundant in
298 mature monomeric Complex IV in both hTim8a$^{MUT\ SH}$ and hTim8b$^{KO\ HEK}$ mitochondria (**Fig 5B-**
299 **C**). By normalising for the total abundance of each protein in each cell line, the change in
300 distribution of Complex IV subunits across assembly stages was assessed (**Fig 5D**). In the
301 absence of hTim8a or hTim8b, COX2 subunits COX5B, COX7B and COX8A were re-
302 distributed to lower intermediates (~200 kDa), which may represent early COX2 module
303 assembly (**Fig 5D**; **Dataset EV5**).

We also observed a pool of COX2 module subunits re-distributed to an assembly at approximately ~280 kDa in hTim8a$^{MUT\ SH}$ mitochondria (**Fig 5D**, top panel, grey box,). The size of this assembly relative to monomeric Complex IV, and the co-migration of COX3 module subunits and assembly factors (MT-CO3, COX7A2, NDUFA4, HIGD2A, PET100 and MR-1S) are consistent with previous complexome studies describing the addition of COX3 module to the S3 subcomplex (**Dataset EV5**) [18]. However, in the absence of hTim8a, the abundances of COX5A, MT-CO2, COX6C, NDUFA4, PET100 and MR-1S were decreased (**Fig 5E**, top panel), suggesting a reduction in S3 subcomplex and perturbation of COX3 module assembly. Although levels of MT-CO3 in this region were unchanged, there was a large increase in HIGD2A which is required for the stability of nascent MT-CO3 [23]. The same region in hTim8b$^{KO\ HEK}$ mitochondria showed a decrease in constituents of the S3 subcomplex (COX4I1, COX5A, MT-CO1, MT-CO2, COX5B and COX6C) in addition to the depletion of COX3 module assembly factors PET100 and MR-1S (**Fig 5E**, bottom panel). These changes were specific to Complex IV, as Complex V and monomeric CIII were unperturbed (**Dataset EV5**). The $CIII_2$-CIV complex was diminished, forcing COX7A2L to associate more with the monomeric CIII as previously reported (**Fig 5D**, ~600 kDa; **Dataset EV5**) [45]. Overall, in cells lacking hTim8a and hTim8b the early intermediates of Complex IV assembly (S2 subcomplex and early COX2 assembly) are stalled. The complexome data suggests the COX2 module is partially able to incorporate into the S3 subcomplex but with decreased efficacy, preventing the efficient addition of COX3 module subunits. We propose the presence of hTim8a and hTim8b supports the efficiency of this step.

Functional overlap of hTim8a and hTim8b in Complex IV biology

The findings above suggest hTim8a and hTim8b are auxiliary assembly factors for building of the S3 subcomplex of Complex IV. We wanted to ascertain if there is functional overlap between the paralogues in this step or in Complex IV biogenesis overall. We attempted to rescue hTim8a$^{MUT\ SH}$ or hTim8b$^{KO\ HEK}$ by expressing the reciprocal paralogue protein. Expression of hTim8b^{FLAG} in hTim8a$^{MUT\ SH}$ cells did not recover the depleted subunits MT-CO1

and MT-CO2, or the assembly factor COX17 (**Fig 6A**). This was confirmed by quantitative proteomics which showed hTim8b^{FLAG} expression did not rescue the loss of subunits from the COX2 (MT-CO2, COX5B, COX6C, COX7C) and COX3 (MT-CO3, COX6B1, COX7A2) modules (**Fig 6B**; **Dataset EV6**), despite COX6B1, COX6C and COX17 being hTim8b^{FLAG} interacting partners (**Fig 1D** and **1F**). hTim8b^{FLAG} was unable to completely recover mature Complex IV compared to wild-type mitochondria as shown by BN-PAGE (**Fig 6C**). Reciprocally, hTim8a^{FLAG} expression in hTim8b$^{KO\ HEK}$ cells was unable to recover mature Complex IV levels on BN-PAGE (**Fig 6D**). Mitochondrial proteomics of hTim8b$^{KO\ HEK}$ cells with and without hTim8a^{FLAG} showed subunits of the COX2 (MT-CO2, COX6C) and COX3 (MT-CO3, COX6A1, COX6B1, NDUFA4) modules were not rescued with hTim8a^{FLAG} expression (**Fig 6E**; **Dataset EV6**), suggesting that both proteins function in Complex IV biogenesis, but potentially at distinct steps in formation of the S3 subcomplex, or under specific cell conditions/requirements.

We next sought to elucidate if the lack of complementation reflected the two paralogues existing in distinct hexameric arrangements with hTim13. Small TIM proteins are stable as heterohexameric assemblies in cells, but it remains unclear whether a complex exists with all three members, or if individual complexes between hTim8a-hTim13 and hTim8b-hTim13 exist in mitochondria. Recombinant hTim8a, hTim8b, and hTim13 were overexpressed and purified by affinity and size-exclusion chromatography (SEC), individually (hTim8a and hTim8b) and as complexes (hTim8a-hTim13 and hTim8b-hTim13) before further SEC analysis. hTim13 could not be purified alone due to its insolubility in the absence of the hTim8a and hTim8b proteins. Comparison of the SEC elution profiles of hTim8a or hTim8b alone with those of the hTim8a-hTim13 and hTim8b-hTim13 complexes (**Fig EV4A-B)** showed that the co-purified proteins eluted as two peaks at ~14.0 and ~15.5 mL. SDS-PAGE (inset **Fig EV4A-B**) showed that hTim8a and hTim8b co-eluted with the hTim13 in the ~14.0 mL peak (fraction 13), indicating complex formation. Attempts to isolate a hTim8a-hTim8b complex by incubation of the corresponding cell lysates prior to purification, yielded a single elution peak (at ~15.5 mL) consistent with the peaks of hTim8a and hTim8b alone (**Figure EV4C**). The addition of purified

hTim8b or hTim8a to pure hTim8a-hTim13 and hTim8b-hTim13 complexes, respectively, did not result in 'exchange' of the hTim8a or hTim8b proteins (to create mixed hTim8a-hTim8b-hTim13 complexes) (insets **Fig EV4D**) or the generation of higher order oligomers (with elution volumes below ~14 mL) (**Fig EV4D**). To identify the complexes observed by SEC, we analysed the singular and co-purified proteins by native and denaturing mass spectrometry (**Fig EV4E-F**). Monomeric protein masses were determined under denaturing conditions (**Fig EV4G**), which enabled the identification of $hTim8a_3$-$hTim13_3$ and $hTim8b_3$-$hTim13_3$ hexamers (each with 3:3 stoichiometry) under native conditions (**Fig EV4H**). In agreement with the SEC results, no complexes larger than hexamer size were detected nor was the presence of mixed hTim8a-hTim8b-hTim13 heterohexamers. These results indicate that, *in vitro*, hTim8a and hTim8b do not oligomerise together in isolation and form distinct heterohexameric complexes with hTim13.

To ascertain if this is also the case *in organello* we performed *in vitro* import of [^{35}S]-hTim8a, [^{35}S]-hTim8b and [^{35}S]-hTim13 into mitochondria isolated from HEK293 cells. This showed a complex of approximately 140 kDa (**Fig EV5A**, labelled #), which is larger than the observed mass of the heterohexamers (60-65 kDa) and suggests an alternate arrangement in cells, either a double hexamer or additional protein interactions. To address the nature of hTim8a, hTim8b and hTim13 in this arrangement [^{35}S]-hTim8a and [^{35}S]-hTim8b were incubated with mitochondria isolated from control HEK293 cells, or cells expressing FLAG-tagged versions of the respective partner proteins. [^{35}S]-hTim8a import into control mitochondria or mitochondria expressing $hTim8b^{FLAG}$ or $hTim13^{FLAG}$ showed the ~140 kDa complex. Antibody-shift with anti-FLAG antibodies shifted this complex although only weakly in $hTim8b^{FLAG}$ mitochondria (**Fig EV5B**, right panel). The same was observed for [^{35}S]-hTim8b which indicated interactions with hTim8a and hTim13 in the ~140 kDa complex (**Fig EV5B**, left panel), though a more robust shift was observed in the hTim8b-hTim13 interaction. As a control, import of [^{35}S]-Tim22 into mitochondria from control or $hTim10b^{3xFLAG}$ expressing cells showed a shift of TIM22 with anti-AGK and anti-FLAG antibodies (**Fig EV5C**). In support of an interaction between hTim8 paralogues *in organello*, the endogenous hTim8a complex

388 migrated faster in hTim8b-deficient HEK293 and SH-SY5Y cells (**Fig EV5D**). Finally, siRNA
389 knock-down of hTim13 (**Fig EV5E**) decreased the abundance of the endogenous hTim8a
390 complex, as observed by immunoblot (**Fig EV5F**), and levels of hTim8b by mass spectrometry
391 (**Fig EV5G**; **Dataset EV2**). This suggests hTim8a and hTim8b both require hTim13 for
392 heterohexamer formation, in agreement with SEC analysis (**Fig EV4C**). Alongside the
393 recombinant protein analysis, these data suggest hTim8a and hTim8b form independent
394 heterohexamers that then may only interact in the presence of their common interacting
395 partners as part of the ~140 kDa complex within mitochondria. The data are consistent with
396 hTim8a-hTim13 and hTim8b-hTim13 heterohexamers having unique but complementary
397 functions in the biogenesis of Complex IV.

398

399 **Discussion**

400 We describe a role for the human small TIM proteins hTim8a, hTim8b and hTim13 as auxiliary
401 assembly factors in the assembly of Complex IV; specifically, the formation of the S3
402 subcomplex. The assembly of mature Complex IV relies on >30 assembly factors to bring
403 together both mtDNA and nuclear encoded subunits in addition to the integration of copper
404 and heme co-factors [21]. The current and favoured model of Complex IV assembly suggests
405 that mature Complex IV is assembled from modules built around core membrane subunits.
406 The mtDNA-encoded MT-CO1 (COX1 module /*S1 subcomplex*) combines with a *scaffold* of
407 COX4I1-COX5A to form the *S2 subcomplex*. Independently, MT-CO2 assembles with
408 COX5B, COX6C, COX7B, COX7C and COX8A to create the COX2 module that is then
409 integrated with the S2 subcomplex to create the *S3 subcomplex*. MT-CO3 and COX6A,
410 COX6B, COX7A and NDUFA4 (the COX3 module) are then added to give rise to the mature
411 Complex IV (*S4 monomeric assembly*) [16, 17]. The creation of the S1 and S2 subcomplexes
412 (early stages of biogenesis) are not affected in the absence of hTim8a and hTim8b.
413 Quantitative proteomics of mitochondria lacking either hTim8 protein in either HEK293 or SH-
414 SY5Y cells shows no significant changes to either of the scaffold components COX5A or
415 COX4I1. This contrasts with other systems where mutation or loss of COX1 module assembly

416 factors COA3, COX10 and COX14 leads to loss of MT-CO1, COX4I1 and COX5A [42, 46].
417 Strikingly, hTim8-deficient cells are depleted of COX2 and COX3 subunits and assembly
418 factors, including core subunits of these modules, MT-CO2 and MT-CO3. The loss of MT-
419 CO2, MT-CO3, COX6A1, COX6B1, COX6C, COX7A, and NDUFA4 is also observed across
420 knock-out or patient cells with dysfunctional COA6, COA7, COX16 and COX20 [22, 37, 47,
421 48], highlighting the crucial role of numerous accessory factors in this complicated assembly
422 pathway.

423 COX17-depleted cells served as a model for COX2 mis-assembly and recapitulated the same
424 loss of COX2 and COX3 subunits as in hTim8-deficient cells, albeit more striking in the
425 absence of COX17. COX1 assembly factors were upregulated in mitochondria lacking hTim8
426 proteins or COX17, including CMC1 [49], COA3 [50], COA5 [51], COX15 [52] and SURF1 [42].
427 Accordingly, we observed an accumulation of the COX1 module in the S2 subcomplex across
428 hTim8a, hTim8b and COX17 knock-out cell lines. Additionally, $COX4I1^{FLAG}$ association with
429 the COX1 module assembly factors COX11, COX15, COX19 and SURF1 was enhanced in
430 the absence of COX17, hTim8a or hTim8b suggesting a delay in the progression of this entity.
431 In contrast, $COX4I1^{FLAG}$ enriched subunits and assembly factors of early COX2 module
432 biogenesis (MT-CO2, COX20, SCO1, SCO2, TMEM177) from hTim8-deficient mitochondria
433 whereas these interactions were decreased in $COX17^{MUT\ HEK}$ cells. This showed that, in
434 contrast to COX17, hTim8 proteins are not required for assembly of the COX2 module and
435 was further supported by the *in vitro* import or radiolabelling of COX2 module subunits in
436 hTim8-deficient cells, which showed no assembly defect. Further, lack of COX17 has a striking
437 impact on stability of mature Complex IV by BN-PAGE, whereas the lack of hTim8a or hTim8b
438 presents a milder phenotype. This is unsurprising given the role of COX17 in copper delivery
439 and, as we show, the hTim8 proteins are likely not directly contributing to cofactor integration.
440 However, the depletion of COX17 protein levels in all cell models lacking either hTim8a or
441 hTim8b suggests an interplay between these proteins.

442 Based on the data presented we propose hTim8a or hTim8b function as auxiliary assembly
443 factors in the formation of the Complex IV S3 subcomplex. This entails the merging of the S2

444 subcomplex (consisting of COX1- COX4I1-COX5A) with the independently established COX2
445 module consisting of MT-CO2, COX5B, COX6C, COX7B, COX7C and COX8A. This inference
446 is supported by: (i) the constituents of the COX2 and COX3 modules are reduced in
447 abundance in mitochondria lacking either hTim8a or hTim8b; (ii) immunoprecipitation and
448 STRING analysis of hTim8a, hTim8b and hTim13 common interacting partners shows a
449 cluster of interactions with COX4I1 COX5A, COX6B1 and COX6C, which comprise the S3
450 subcomplex; and (iii) complexome profiling of hTim8-deficient mitochondria revealed a
451 decrease in the levels of the S3 subcomplex, accumulation of S2 subcomplex and perturbation
452 of COX3 assembly, indicating the maintenance of competent S3 subcomplex is less
453 efficacious. The assembly of Complex IV requires that subcomplexes and core subunits are
454 stabilised until later modules are added as in the case of SMIM20 (MITRAC7), which prevents
455 COX1 turnover until the addition of COX2 module [53], and TMEM177, required for the
456 maturation and stability of nascent MT-CO2 [40]. We show that in the absence of hTim8
457 proteins, the translation and stability of mtDNA-encoded core subunits (MT-CO1, MT-CO2
458 and MT-CO3) is not influenced. However, akin to SMIM20, the interaction of hTim8-hTim13
459 chaperone complexes might help stabilise the COX2 module in the S3 subcomplex, awaiting
460 the subsequent addition of the COX3 module. The current data cannot distinguish whether
461 hTim8-hTim13 complexes recruit the assembled COX2 module to the S3 subcomplex or act
462 to stabilise the S3 subcomplex after COX2 module integration, preventing dissociation or
463 turnover, but both are reasonable options worthy of exploration. Even though a proportion of
464 monomeric Complex IV and S3 subcomplex persist in hTim8-deficient cells, loss of SURF1
465 (involved in the S2-to-S3 transition) in patient cells displays a similar decrease but not
466 complete ablation of monomeric Complex IV [43], suggesting there might be redundancy in
467 this system with numerous factors acting at discrete sites.

468 Unlike other respiratory chain complexes, Complex IV has multiple tissue-specific subunits
469 and alternate isoforms [54-56]. These isoforms can drive adaptations, such as improved
470 Complex IV activity in hypoxia [57], necessary for specialised cell types or the tissue
471 environment. We previously observed cell-specific differences in the metabolism and survival

of hTim8-deficient cells [15]. Our data suggests the paralogues have distinct functions, which is consistent with only hTim8a being associated with a neurological mitochondrial disease (MTS) [15]. Indeed, our previous work showed that only hTim8a-deficient cells displayed increased levels of cytochrome *c* and apoptotic sensitivity driven by redox stress associated with Complex IV dysfunction. Importantly, while cells lacking hTim8b have reduced levels of COX17 they do not display apoptotic sensitivity as observed in hTim8a cells, reiterating cell-specific function of the paralogues and/or unique functions. How the functions of hTim8a and hTim8b are supported by the arrangement of these proteins within heterohexameric assemblies warrants further investigation. We show that both hTim8a and hTim8b proteins rely on hTim13 for heterohexamer formation, but do not interact together as a hTim8a-hTim8b heterohexamer *in vitro*. In mitochondria, both western blotting and *in vitro* import analysis of the individual hTim8 proteins showed assembly into a ~140 kDa complex, quite distinct from the expected 60-65 kDa of the heterohexamers. Antibody-shift analysis suggests that hTim8a can interact with both hTim8b and hTim13 in this ~140 kDa species, implying an alternate arrangement in cells to what is observed *in vitro*; either a double hexamer or indeed additional common protein interactions with those detected here in immunoprecipitation analysis. Whether this complex is the functional species facilitating Complex IV assembly cannot be speculated with the data at hand.

In summary, we propose a novel function of hTim8a, hTim8b and hTim13 in the assembly of Complex IV as auxiliary assembly factors/chaperones for the formation of S3 subcomplex.

Materials and Methods

Human cell lines and culturing conditions, stable cell line generation, siRNA transfection

Cell lines used in this study include: HEK293T (RRID: CVCL_0063), HEK Flp-In T-REx (ThermoFisher Scientific; RRID: CVCL_U427), SH-SY5Y (RRID: CVCL_0019). CRISPR/Cas9 knock-out cell lines edited for *TIMM8A* (HEK293 and SH-SY5Y) and *TIMM8B* (HEK293 and SH-SY5Y) were described previously [15]. Parental lineages have been authenticated and all cell lines were free from mycoplasma contamination. Cells were cultured in Dulbecco's modified Eagle's medium (DMEM, Gibco) supplemented with 5% or 10% [v/v] foetal bovine serum (FBS; In vitro Technologies), and 0.01% [v/v] penicillin-streptomycin at 37°C and with 5% atmospheric CO_2. Tetracycline inducible HEK Flp-In T-REx 293 stable cell lines were generated according to the manufacturer's instructions. Lentiviral and retroviral transduction (of hTim8b^{FLAG} and COX4I1^{FLAG}) was undertaken as previously described [15] using pLVX-TetOne-[ORF]-Puro or pBMN-[ORF]-Puro plasmids with the packaging plasmids pVSVG and pSPAX2. siRNA targeting Yme1L (5' CGAAUUUGAUGAGAUGUUU[dT][dT] 3') and hTim13 (5' CAAGUGUUUCCGGAAGUGU[dT][dT] 3'), or control scrambled siRNA (Sigma-Aldrich) were transfected into HEK Flp-In T-REx 293 cells using DharmaFECT (Dharmacon). 10 nM of siRNA was transfected into cells. 46 h post transfection cells were transfected with another 10 nM of siRNA and then harvested a total 72 h after initial transfection. For proteasome inhibition, cells were treated with 5 μM MG132 in DMSO for timepoints up to 6 h.

CRISPR/Cas9 gene editing and screening

The pSpCas9(sgRNA)-2A-GFP plasmid (Addgene #48138) encoding short guide RNA (sgRNA) targeting exon 1 of *COX17* was transfected into cells prior to single-cell sorting (FACSAria^{TM} III sorter, BD Biosciences) by GFP fluorescence [58]. Individual clones were expanded and screened by immunoblotting for the presence of COX17. The *COX17* locus was refractory to PCR amplification, so the loss or modification of COX17 in candidate clones was interrogated by tandem mass spectrometry.

525 **Whole cell lysis, mitochondrial isolation, and cellular fractionation**

526 Cell pellets were resuspended in lysis buffer (150 mM NaCl, 1% [v/v] TritonX-100, 0.1% [w/v]
527 SDS, 10 mM Tris pH 7.5, 5 mM EDTA, 1x complete protease inhibitor (Roche)) and incubated
528 on ice for 20 min. Lysates were clarified at 16,000 *g* for 10 min at 4°C. Mitochondrial isolation
529 was performed as previously described [24]. Cytosolic fractions were obtained by
530 centrifugation of the post-mitochondrial supernatant at 100,000 *g* for 30 min at 4°C. For
531 membrane protein extraction, isolated mitochondria were resuspended in 100 mM Na_2CO_3 pH
532 9.0 and incubated for 30 min on ice. Pellet and supernatant fractions were separated by
533 centrifugation at 100,000 *g* for 30 min at 4°C. Protein quantitation was achieved using Pierce™
534 BCA protein assay kit (ThermoFisher Scientific).

535 ***In vitro* protein import**

536 mRNA encoding targets of interest was created using mMessage mMachine SP6 transcription
537 kit (Ambion) according to the manufacturer's instructions. Cell-free translation of proteins was
538 undertaken in rabbit reticulocyte lysate (Promega) using [^{35}S]-methionine as per
539 manufacturer's instruction. Isolated mitochondria were resuspended to 1 mg/mL in import
540 buffer (20 mM HEPES-KOH pH 7.4, 250 mM sucrose, 5 mM magnesium acetate and 80 mM
541 magnesium acetate) supplemented with 10 mM sodium succinate, 1 mM 1,4-dithiothreitol and
542 5 mM ATP, then incubated at 37°C prior to the addition of radiolabelled proteins. Proteinase
543 K was added at 50 µg/mL and incubated for 10 min on ice, followed by 1 mM PMSF for 5 min
544 on ice. Samples were processed for SDS-PAGE or BN-PAGE analysis; SDS-PAGE samples
545 were precipitated with 12.5% [v/v] trichloroacetic acid prior to the addition of SDS-PAGE
546 loading dye. For antibody-shift analysis, 1 µL of antibody was added to each sample during
547 the solubilisation step of BN-PAGE preparation. Gels were transferred to PVDF membrane
548 before exposure of the radioactive signal to a phosphorimager screen (Cytiva), which was
549 detected using an Amersham Typhoon Biomolecular Imager (Cytiva).

550 **Radiolabelling of mitochondrial translation products**

Cells were cultured for radiolabelling as previously described [22]. Briefly, cells were labelled in Met/Cys-free DMEM (Life Technologies), supplemented with 10% [v/v] dialysed FBS (GE Healthcare), 0.01% [v/v] penicillin-streptomycin, 1 mM sodium pyruvate, 1×GlutaMAX (Life Technologies), 50 µg/mL uridine, 7 µg/mL anisomycin (Sigma Aldrich), and 7 µCi [^{35}S]-Met/Cys (PerkinElmer) and labelled for 2 h. Labelling was quenched with 10 µM "cold" methionine and labelling media was replaced with standard DMEM media for 0, 3, or 24 h. Mitochondria isolated from radiolabelled cells were analysed by SDS-PAGE and transferred to PVDF membrane before exposure of the radioactive signal to a phosphorimager screen (Cytiva) and detection using an Amersham Typhoon Biomolecular Imager (Cytiva).

Immunoprecipitation and crosslinking

Isolated mitochondria were solubilised at 2 mg/mL in solubilisation buffer (20 mM Tris-Cl pH 7.4, 50 mM NaCl, 0.1 mM EDTA, 10% [v/v] glycerol) supplemented with 1% [w/v] digitonin and 1x protease inhibitor. Lysates were mixed end-over-end at 4°C for 30 min and clarified at 16,000 *g* for 30 min at 4°C. Lysates were diluted 1:10 [v/v] solubilisation buffer (to final 0.1% digitonin) and applied to equilibrated M2 anti-FLAG resin (Sigma-Aldrich) and mixed end-over-end at 4°C for 1.5 h. The resin was washed with x4 500 µL volumes of solubilisation buffer (with 0.1% digitonin), followed by elution in x2 100 µL volumes of 0.2 M glycine, pH 2.0. For DSP crosslinking and immunoprecipitation, isolated mitochondria were resuspended at 1 mg/mL in import buffer (with 5 mM ATP) and either 0.2 mM DSP (ThermoFisher Scientific) or DMSO alone and crosslinked for 1 h at 4°C, mixing end-over-end, after which the reaction was quenched with 100 mM Tris-Cl, pH 7.4 for 30 min on ice. Mitochondrial pellets were solubilised at 2.5 mg/mL in SDS lysis buffer (20 mM Tris-Cl, pH 7.4, 1 mM EDTA, 1% [w/v] SDS) by heating at 95°C for 15 min. The supernatant was clarified by centrifugation, diluted 1:10 [v/v] in TritonX-100 buffer (1% [v/v] TritonX-100, 20 mM Tris-Cl pH 7.4, 150 mM NaCl, 1 X cOmplete protease inhibitor), and applied to equilibrated M2 anti-FLAG resin with end-over-end mixing at 4°C for 1.5 h. The resin was washed with x4 500 µL volumes of TritonX-100 buffer, followed by elution in x2 100 µL volumes of 0.2 M glycine, pH 2.0.

Protein gel electrophoresis and immunoblot analysis

Tris-Tricine SDS-PAGE was performed as detailed previously [24, 59]. Acrylamide stock solution (49.5% [w/v] acrylamide, 1.5% [w/v] bisacrylamide) was diluted in tricine buffer (1 M Tris-Cl pH 8.45, 0.1% [w/v] SDS) to make 10% and 16% acrylamide gel mixes, with 13% [v/v] glycerol added to the latter. 10-16% acrylamide separating gel was overlayed with a 4% acrylamide (in tricine buffer) stacking gel. SDS-PAGE loading dye (50 mM Tris-Cl pH 6.8, 100 mM 1,4-dithiothreitol, 2% [w/v] sodium dodecyl sulphate, 10% [v/v] glycerol, 0.1% [w/v] bromophenol blue) was added to samples prior to heating at 95°C for 5 min; or 50°C for 15 min for analysis of core OXPHOS subunits. Electrophoresis was performed in Tris-tricine SDS-PAGE cathode buffer (0.1 M Tris, 0.1 M Tricine pH 8.45, 0.1% SDS) and anode buffer (0.2 M Tris-Cl pH 8.9).

Blue native-PAGE (BN-PAGE) was performed as previously described [15]. Acrylamide stock solution was diluted in blue native gel buffer (66 mM α-amino n-caproic acid, 50 mM Bis-Tris pH 7.0) to create 4% and 16% acrylamide gel mixes, with 13% glycerol added to the latter. A 4-16% acrylamide gradient separating gel was poured by gradient mixer and a 4% acrylamide stacking gel overlayed on top. Isolated mitochondria were solubilised in solubilisation buffer (20 mM Tris-Cl pH 7.4, 50 mM NaCl, 0.1 mM EDTA and 10% [v/v] glycerol) plus 1% [w/v] digitonin and incubated on ice for 30 min. The samples were clarified by centrifugation and the supernatant added to blue native loading dye (0.5% [w/v] Coomassie blue G250 (MP Biomedicals, LLC), 50 mM α-amino n-caproic acid, 10 mM Bis-Tris pH 7.0). Electrophoresis was carried out using blue native cathode buffer (50 mM tricine, 15 mM Bis-Tris pH 7.0, 0.02% [w/v] Coomassie blue G 250) and anode buffer (50 mM Bis-Tris pH 7.0). Gels were transferred to 0.45 µm polyvinylidene fluoride (PVDF) membranes by semi-dry transfer. Immunoblotting employed primary antibodies, detailed in the resource table (**Appendix**), and horse radish peroxidase-conjugated secondary antibodies (Sigma-Aldrich). Signal was generated by Clarity Western ECL Substrate (BioRad) and imaged using a ChemiDoc™ MP imaging machine (BioRad). Image processing and quantification was done in ImageLab software (BioRad).

Hydrogen peroxide measurement

H_2O_2 released by cells into the culture media was measured by ROS-Glo™ H_2O_2 Assay (Promega). Briefly, $4x10^4$ cells were seeded in triplicate in 96-well plates. After 24 h growth, the provided H_2O_2 dilution buffer and luciferin precursor substrate were added with either 10 µM menadione or DMSO (vehicle alone) and incubated at 37°C for 2 h. The addition of detection solution was followed by a 20 min incubation in the dark at room temperature. Luminescence was measured using FLUOstar OPTIMA microplate reader (BMG LABTECH). An unpaired two-tailed Student's t-test was employed for hypothesis testing.

Complexome profiling

Control and knock-out cells were isotopically labelled in SILAC media (Arg/Lys-free DMEM, 10% [v/v] dialysed FBS, 0.01% [v/v] penicillin-streptomycin, 1 mM sodium pyruvate, 1×GlutaMAX, 50 µg/mL uridine) containing 'light' ($^{12}C_6{}^{14}N_4$-arginine, $^{12}C_6{}^{14}N_2$-lysine) or 'heavy' ($^{13}C_6{}^{15}N_4$-arginine, $^{13}C_6{}^{15}N_2$-lysine) amino acids for 2 weeks (~6 doublings). Mitochondria isolated from SILAC-labelled cells were prepared in 100 µg aliquots. Heavy- and light-labelled aliquots were combined and separated by BN-PAGE. Protein complexes were fixed by soaking the gel in 50% [v/v] carbonyl-free methanol, 10% [v/v] acetic acid, 10 mM ammonium acetate for 30 min at RT. Proteins were stained in Coomassie gel solution (0.025% [w/v] Coomassie blue G250, 10% acetic acid) for 30 min at RT and then destained in 10% acetic acid overnight. The gel was washed thrice in dH_2O prior to excising and slicing the lane into 60 even slices. Each slice was minced and transferred to 50 mM ammonium bicarbonate (ABC) in a filtered microtitre plate (30-40 µM PP/PE, Acroprep™) before proceeding with in-gel digestion as described below.

Peptide digestion and clean-up for mass spectrometry

Isolated mitochondria were solubilised, reduced, and alkylated in SDC buffer (1% [w/v] sodium deoxycholate, 100 mM Tris-Cl pH 8.1, 40 mM chloroacetamide, 10 mM tris(2-carboxyethyl)phosphine (TCEP)) by first boiling at 99°C for 5 min with 1500 rpm shaking, then sonication (Powersonic 603 Ultrasonic Cleaner, 40 KHz on high power) for 15 min at room temperature. Proteins were digested with 1:50 [w/w; trypsin:protein] trypsin (ThermoFisher

Scientific) for 4-6 h at 37°C, then clarified by centrifugation. Peptides were loaded onto stage-tips [60] with x3 plugs of SDB-RPS substrate (3M™Empore™) in the presence of isopropanol with 1% [v/v] trifluoroacetic acid (TFA). Sample binding and subsequent washing was achieved by centrifugation at 2,500 *g*. Peptides were washed first in isopropanol, 1% TFA, and then 0.2% [v/v] TFA, before being eluted in 80% [v/v] acetonitrile (ACN), 1% [v/v] ammonium hydroxide. Eluates were lyophilised by CentriVap SpeedVac concentrator (Labconco) or Modulyo D-230 freeze-dryer (Thermo Electron) and reconstituted in 0.1% [v/v] TFA, 2% [v/v] ACN for analysis.

Immunoprecipitation eluates and MG132 or sodium carbonate treated fractions were acetone-precipitated and then solubilised in 8 M urea, 50 mM ABC pH 8.0, by vortex and sonication for 15 min. Reduction and alkylation was achieved with 5 mM TCEP, 50 mM chloroacetamide and incubation at 37°C with 700 RPM shaking for 30 min. Urea content was diluted to 1 M by addition of 50 mM ABC and 1 µg of trypsin was added to incubate overnight at 37°C. Stage-tips were created with SDB-XC substrate (x2 plugs for eluates, x6 plugs for fractions; 3M™Empore™) and activated with 100% ACN, then equilibrated with 0.1% TFA, 2% ACN. The addition of TFA (1% [v/v] final concentration) acidified the peptides prior to their loading on stage-tips. Stage-tips were washed twice with 0.1% TFA, 2% ACN and peptides eluted in 0.1% [v/v] TFA, 80% [v/v] ACN. Eluates were lyophilised by CentriVap SpeedVac concentrator (Labconco) or Modulyo D-230 freeze-dryer (Thermo Electron) and reconstituted in 0.1% [v/v] TFA, 2% [v/v] ACN for analysis.

Proteins for complexome analysis were subject to in-gel digestion as described previously [61]. The minced samples were centrifuged at 1,500 *g* for 3 min at RT and destained in 60% [v/v] carbonyl-free methanol, 50 mM ABC for 1 h at RT with 500 RPM shaking. Destaining was repeated twice, with 15 min incubations. Samples were washed in 50% [v/v] ACN, 50 mM ABC, reduced by incubation in 10 mM DTT, 50 mM ABC at 56°C for 1 h, and then alkylated in 40 mM chloroacetamide, 50 mM ABC for 45 min at RT. Samples were washed twice in 50% ACN, 50 mM ABC and left to air-dry in the plate. Once dry, 20 µL of digestion solution (10 ng/µL MS-grade trypsin (ThermoFisher Scientific), 10 % [v/v] ACN, 0.01% [w/v] ProteaseMAX

surfactant (Promega), 1 mM $CaCl_2$, 50 mM ABC) was added to each well and allowed to swell for 10 min at 4°C. An additional 80 µL of 50 mM ABC was added, followed by overnight incubation at 37°C in a pre-humidified incubator. Peptides were eluted by centrifugation at 1,500 *g* for 3 min at RT and subsequent addition of 30% ACN, 3% FA and centrifugation. Peptide elutions were lyophilised in CentriVap SpeedVac concentrator (Labconco) then reconstituted in 2% ACN, 0.1% TFA. Peptides were then desalted using SDB-XC staged-tips and prepared for analysis as described for immunoprecipitation samples.

LC-MS/MS machine methods and data analysis pipeline are described in the **Appendix**.

Inductively coupled plasma-mass spectrometry

Intact cells and isolated mitochondria were isolated, in triplicate, as 100 µg samples. Each sample was digested in 200 µL 35% [v/v] nitric acid (HNO_3, Suprapur, Merck) at 96°C for 20 min. Samples were diluted to a final volume of 1 mL using MilliQ-H_2O and centrifuged at 20,000 *g* for 25 min. All elemental analyses were performed using an Agilent 8900 Triple Quadrupole ICP-MS (Agilent Technologies) using a MicroMist nebulizer (Glass Expansion, Australia) with instrument parameters detailed in **Dataset EV4**. Torch positioning, sample depth adjustment and lens optimisation were set according to manufacturer recommendations while the other instrumental parameters were optimized during a batch-specific user tune prior to each experimental run (**Dataset EV4**). The mass spectrometer was calibrated for magnesium (Mg), calcium (Ca), manganese (Mn), iron (Fe), copper (Cu), zinc (Zn) and cadmium (Cd) using 0, 10, 25, 50, 100, 250 & 500 µg/L mixed multi-element standard calibration solutions in standard diluent from commercially available (Multi-element Calibration Standard 2A) certified reference standards (Agilent Technologies). A reference elemental solution containing 100 µg/L yttrium (Y) in standard (Agilent Technologies) was used to normalize all measurements.

Copper binding assay

The binding affinities of the hTim8a, hTim8b and COA6 proteins for Cu(I) were measured as previously described [37]. Briefly, purified proteins (in 20 mM Tris-MES pH 8.0) were titrated

689 at increasing concentrations (0 – 30 μM) into solutions containing buffer (20 mM Tris-MES pH
690 8.0), $CuSO_4$ (20 μM), BCS (200 μM) and NH_2OH (1 mM). The transfer of Cu(I) from the
691 $[Cu^{I}BCS_2]^{3-}$ complex to protein samples was monitored by measuring the absorbance of
692 solutions at 483 nm, using a CLARIOstar plate reader (BMG Labtech). $[Cu^{I}BCS_2]^{3-}$ complex
693 concentrations were determined using absorbance values at 483 nm and plotted against
694 protein:Cu ratios. Data was fit using Kaleidagraph software (version 4) and the copper binding
695 affinities calculated as previously described [37, 62]. Plots were visualised using Prism
696 GraphPad software (version 9).

697 **Expression and purification of recombinant small TIM proteins**

698 *Escherichia coli* strain SHuffle T7 (New England Biolabs) were transformed with pGEX-6P-1
699 plasmids with ORFs encoding the hTim8a, hTim8b and hTim13 proteins. Cultures were grown
700 in Luria Broth supplemented with ampicillin (100 μg/mL), chloramphenicol (35 μg/mL) and
701 streptomycin (50 μg/mL) at 30˚C to an OD600 of 0.6-0.8, then induced with IPTG (0.2 mM)
702 and incubated with shaking for 16 h at 16˚C. Cells were harvested by centrifugation at 8000
703 *g*, 15 min, 4˚C and stored at -20˚C until use. Recombinant hTim8a, hTim8b and hTim13 were
704 purified by a two-step protocol consisting of glutathione (GSH) affinity and size-exclusion
705 chromatography (SEC). Cell pellets were suspended in PBS (pH 7.4) containing 1x cOmplete
706 protease inhibitor (Sigma-Aldrich) and lysed using a TS series bench top cell disrupter
707 (Constant System Ltd) at 35 kpsi, followed by centrifugation at 30000 *g*, 30 min, 4˚C. The
708 supernatant was incubated with Sepharose 4B resin (Cytiva) that had been pre-equilibrated
709 with PBS (3 h, 4˚C). Unbound protein was eluted following incubation, and resin-bound protein
710 incubated overnight (4˚C) with 3C PreScission Protease to cleave the glutathione s-
711 transferase (GST) tag. Cleavage of the GST tag introduced five residues (GPLGS) to the N-
712 termini of the proteins. Cleaved proteins were further purified using size-exclusion
713 chromatography (HiLoad 16/600 Superdex 75 pg (Cytiva), 50 mM Tris-Cl pH 8.0 and 150 mM
714 NaCl). The hTim13 precipitated from solution after GST-tag cleavage and could not be further
715 purified. For the preparation of the hTim8a-hTim13 and hTim8b-hTim13 complexes, cells
716 expressing hTim13 were disrupted, and debris cleared by centrifugation before combining with

cleared lysates from the hTim8a or hTim8b overexpressions in equal volumes. The purification of the hTim8a-hTim13 and hTim8b-hTim13 complexes proceeded as described above for the hTim8a and hTim8b proteins. Unsuccessful attempts to co-purify a hTim8a-hTim8b complex followed the same protocol. Purified proteins were concentrated to 10 mg/mL and stored at -80˚C until use.

Size-exclusion chromatography

Pure samples of hTim8a, hTim8a, the hTim8a-hTim13 and hTim8b-hTim13 complexes were prepared as described above. These samples were analysed by analytical SEC (Superdex S200 Increase 10/300 GL (Cytiva), 50 mM Tris-Cl pH 8.0 and 150 mM NaCl). Mixtures of hTim8a with the hTim8b-hTim13 complex and hTim8b with the hTim8a-hTim13 complex were incubated on ice (1 h), so that the hTim8a:hTim8b was at approximate molar equivalence. The samples were then reseparated by analytical SEC (as above). Fractions from the SEC step were analysed by SDS-PAGE. Chromatography traces and SDS-PAGE analyses were used in combination to assess oligomerisation activity.

Experimental design and statistical rationale

Label-free quantitative LC-MS/MS methods and statistical treatments were consistent with published analyses employing similar instrumentation and protocols [23, 37]. All mass spectrometry experiments were performed in n=3 biological replicates for each experimental condition and compared to n=3 biological replicates of the relevant control (wild-type cells, non-crosslinked, vehicle treated, or scramble siRNA). The log_2-transformed LFQ intensity data fit a normal distribution and statistical significance of fold change differences was determined by unpaired two-sided t-test with permutation-based FDR for multiple hypothesis testing. Replicates were sufficiently concordant to achieve significance with n=3 samples. Differences in purity of mitochondrial isolates were accounted for by global row normalisation and fractionated samples were analysed independently (for MG132 treatment) or normalised for ‘total protein abundance’ using samples taken prior to fractionation (for sodium carbonate treatment). Random error was further mitigated by minimum LFQ count in the search

parameters and a threshold of ≥2 unique peptides identified in ≥2 experimental replicates for the application of a t-test. Additional search and statistical parameters are described in the **Appendix**. Mass spectrometric analyses were validated by parallel methods where appropriate/possible.

Please see Appendix for: *LC-MS/MS*; *Data Analysis*; *Antibodies.*

Data availability

The mass spectrometry proteomics data have been deposited to the ProteomeXchange Consortium, via the PRIDE partner repository, with the dataset identifier PXD037906 (https://www.ebi.ac.uk/pride/archive/projects/PXD037906).

Acknowledgements

We acknowledge support from the Mito Foundation to the Stojanovski Lab (Incubator and Booster Grant). AJA, JC and MeJB are supported by Australian Government RTP Scholarships and Mito Foundation top-up scholarships. MJM acknowledges funding by the Australian Research Council (ARC) Future Fellowship (FT180100397), Discovery Project Grant (DP220102030) and NHMRC Project Grant (GNT1165217; to MTR and MJM). LEF acknowledges support from the Mito Foundation and the NHMRC (Investigator Grant 2010149). We thank the University of Melbourne Mass Spectrometry and Proteomics Facility, Biological Optical Microscopy Platform and Flow Cytometry Platform. AUC analyses were carried out by Dr Yee-Foong Mok at Melbourne Protein Characterization Facility (Bio21). We thank Ms Ellanor Goyne for contributions to protein production; Dr Shadi Maghool for assistance with the Cu(I)-binding assay; A/Prof. David Stroud (University of Melbourne) for discussion and reagents.

Conflict of interest

The authors have no conflicts of interest to declare.

References

1. Curran SP, Leuenberger D, Schmidt E, Koehler CM (2002) The role of the Tim8p-Tim13p complex in a conserved import pathway for mitochondrial polytopic inner membrane proteins. *J Cell Biol* **158**: 1017-27
2. Koehler CM, Jarosch E, Tokatlidis K, Schmid K, Schweyen RJ, Schatz G (1998) Import of mitochondrial carriers mediated by essential proteins of the intermembrane space. *Science* **279**: 369-73
3. Leuenberger D, Bally NA, Schatz G, Koehler CM (1999) Different import pathways through the mitochondrial intermembrane space for inner membrane proteins. *The EMBO journal* **18**: 4816-4822
4. Beverly KN, Sawaya MR, Schmid E, Koehler CM (2008) The Tim8–Tim13 Complex Has Multiple Substrate Binding Sites and Binds Cooperatively to Tim23. *Journal of Molecular Biology* **382**: 1144-1156
5. Hoppins SC, Nargang FE (2004) The Tim8-Tim13 complex of Neurospora crassa functions in the assembly of proteins into both mitochondrial membranes. *J Biol Chem* **279**: 12396-405
6. Weinhäupl K, Lindau C, Hessel A, Wang Y, Schutze C, Jores T, Melchionda L, Schonfisch B, Kalbacher H, Bersch B*, et al.* (2018) Structural Basis of Membrane Protein Chaperoning through the Mitochondrial Intermembrane Space. *Cell* **175**: 1365-1379 e25
7. Paschen SA, Rothbauer U, Káldi K, Bauer MF, Neupert W, Brunner M (2000) The role of the TIM8-13 complex in the import of Tim23 into mitochondria. *The EMBO journal* **19**: 6392-6400
8. Weinhäupl K, Wang Y, Hessel A, Brennich M, Lindorff-Larsen K, Schanda P (2021) Architecture and assembly dynamics of the essential mitochondrial chaperone complex TIM9·10·12. *Structure* **29**: 1065-1073.e4
9. Bauer MF, Rothbauer U, Mühlenbein N, Smith RJH, Gerbitz K-D, Neupert W, Brunner M, Hofmann S (1999) The mitochondrial TIM22 preprotein translocase is highly conserved throughout the eukaryotic kingdom. *FEBS Letters* **464**: 41-47
10. Munoz-Gomez SA, Snyder SN, Montoya SJ, Wideman JG (2020) Independent accretion of TIM22 complex subunits in the animal and fungal lineages. *F1000Res* **9**: 1060
11. Roesch K, Hynds PJ, Varga R, Tranebjaerg L, Koehler CM (2004) The calcium-binding aspartate/glutamate carriers, citrin and aralar1, are new substrates for the DDP1/TIMM8a-TIMM13 complex. *Hum Mol Genet* **13**: 2101-11
12. Jin H, May M, Tranebjærg L, Kendall E, Fontán G, Jackson J, Subramony SH, Arena F, Lubs H, Smith S*, et al.* (1996) A novel X–linked gene, DDP, shows mutations in families with deafness (DFN–1), dystonia, mental deficiency and blindness. *Nature Genetics* **14**: 177-180
13. Hofmann S, Rothbauer U, Muhlenbein N, Neupert W, Gerbitz KD, Brunner M, Bauer MF (2002) The C66W mutation in the deafness dystonia peptide 1 (DDP1) affects the formation of functional DDP1.TIM13 complexes in the mitochondrial intermembrane space. *J Biol Chem* **277**: 23287-93
14. Rothbauer U, Hofmann S, Mühlenbein N, Paschen SA, Gerbitz KD, Neupert W, Brunner M, Bauer MF (2001) Role of the deafness dystonia peptide 1 (DDP1) in import of human Tim23 into the inner membrane of mitochondria. *J Biol Chem* **276**: 37327-34
15. Kang Y, Anderson AJ, Jackson TD, Palmer CS, De Souza DP, Fujihara KM, Stait T, Frazier AE, Clemons NJ, Tull D*, et al.* (2019) Function of hTim8a in complex IV assembly in neuronal cells provides insight into pathomechanism underlying Mohr-Tranebjaerg syndrome. *Elife* **8**
16. Brischigliaro M, Zeviani M (2021) Cytochrome c oxidase deficiency. *Biochimica et Biophysica Acta (BBA) - Bioenergetics* **1862**: 148335
17. Nijtmans LGJ, Taanman J-W, Muijsers AO, Speijer D, Van den Bogert C (1998) Assembly of cytochrome-c oxidase in cultured human cells. *European Journal of Biochemistry* **254**: 389-394

18. Vidoni S, Harbour ME, Guerrero-Castillo S, Signes A, Ding S, Fearnley IM, Taylor RW, Tiranti V, Arnold S, Fernandez-Vizarra E*, et al.* (2017) MR-1S Interacts with PET100 and PET117 in Module-Based Assembly of Human Cytochrome c Oxidase. *Cell Reports* **18**: 1727-1738
19. Lim Sze C, Smith Katherine R, Stroud David A, Compton Alison G, Tucker Elena J, Dasvarma A, Gandolfo Luke C, Marum Justine E, McKenzie M, Peters Heidi L*, et al.* (2014) A Founder Mutation in PET100 Causes Isolated Complex IV Deficiency in Lebanese Individuals with Leigh Syndrome. *The American Journal of Human Genetics* **94**: 209-222
20. Stiburek L, Vesela K, Hansikova H, Pecina P, Tesarova M, Cerna L, Houstek J, Zeman J (2005) Tissue-specific cytochrome c oxidase assembly defects due to mutations in SCO2 and SURF1. *Biochem J* **392**: 625-32
21. Timon-Gomez A, Nyvltova E, Abriata LA, Vila AJ, Hosler J, Barrientos A (2018) Mitochondrial cytochrome c oxidase biogenesis: Recent developments. *Semin Cell Dev Biol* **76**: 163-178
22. Formosa LE, Maghool S, Sharpe AJ, Reljic B, Muellner-Wong L, Stroud DA, Ryan MT, Maher MJ (2022) Mitochondrial COA7 is a heme-binding protein with disulfide reductase activity, which acts in the early stages of complex IV assembly. *Proc Natl Acad Sci U S A* **119**
23. Hock DH, Reljic B, Ang CS, Muellner-Wong L, Mountford HS, Compton AG, Ryan MT, Thorburn DR, Stroud DA (2020) HIGD2A is Required for Assembly of the COX3 Module of Human Mitochondrial Complex IV. *Mol Cell Proteomics* **19**: 1145-1160
24. Kang Y, Baker MJ, Liem M, Louber J, McKenzie M, Atukorala I, Ang C-S, Keerthikumar S, Mathivanan S, Stojanovski D (2016) Tim29 is a novel subunit of the human TIM22 translocase and is involved in complex assembly and stability. *eLife* **5**: e17463
25. Szklarczyk D, Gable AL, Nastou KC, Lyon D, Kirsch R, Pyysalo S, Doncheva NT, Legeay M, Fang T, Bork P*, et al.* (2020) The STRING database in 2021: customizable protein–protein networks, and functional characterization of user-uploaded gene/measurement sets. *Nucleic acids research* **49**: D605-D612
26. Al-Habib H, Ashcroft M (2021) CHCHD4 (MIA40) and the mitochondrial disulfide relay system. *Biochem Soc Trans* **49**: 17-27
27. Geldon S, Fernández-Vizarra E, Tokatlidis K (2021) Redox-Mediated Regulation of Mitochondrial Biogenesis, Dynamics, and Respiratory Chain Assembly in Yeast and Human Cells. *Frontiers in cell and developmental biology* **9**: 720656
28. Habich M, Salscheider SL, Murschall LM, Hoehne MN, Fischer M, Schorn F, Petrungaro C, Ali M, Erdogan AJ, Abou-Eid S*, et al.* (2019) Vectorial Import via a Metastable Disulfide-Linked Complex Allows for a Quality Control Step and Import by the Mitochondrial Disulfide Relay. *Cell Rep* **26**: 759-774 e5
29. Petrungaro C, Zimmermann KM, Küttner V, Fischer M, Dengjel J, Bogeski I, Riemer J (2015) The Ca(2+)-Dependent Release of the Mia40-Induced MICU1-MICU2 Dimer from MCU Regulates Mitochondrial Ca(2+) Uptake. *Cell Metab* **22**: 721-33
30. Bragoszewski P, Gornicka A, Sztolsztener ME, Chacinska A (2013) The ubiquitin-proteasome system regulates mitochondrial intermembrane space proteins. *Mol Cell Biol* **33**: 2136-48
31. Bragoszewski P, Turek M, Chacinska A (2017) Control of mitochondrial biogenesis and function by the ubiquitin-proteasome system. *Open Biol* **7**
32. MacVicar T, Ohba Y, Nolte H, Mayer FC, Tatsuta T, Sprenger H-G, Lindner B, Zhao Y, Li J, Bruns C*, et al.* (2019) Lipid signalling drives proteolytic rewiring of mitochondria by YME1L. *Nature* **575**: 361-365
33. Hangen E, Feraud O, Lachkar S, Mou H, Doti N, Fimia GM, Lam NV, Zhu C, Godin I, Muller K*, et al.* (2015) Interaction between AIF and CHCHD4 Regulates Respiratory Chain Biogenesis. *Mol Cell* **58**: 1001-14
34. Zong S, Wu M, Gu J, Liu T, Guo R, Yang M (2018) Structure of the intact 14-subunit human cytochrome c oxidase. *Cell Research* **28**: 1026-1034

35. Jett KA, Leary SC (2018) Building the CuA site of cytochrome c oxidase: A complicated, redox-dependent process driven by a surprisingly large complement of accessory proteins. *J Biol Chem* **293**: 4644-4652
36. Banci L, Bertini I, Ciofi-Baffoni S, Hadjiloi T, Martinelli M, Palumaa P (2008) Mitochondrial copper(I) transfer from Cox17 to Sco1 is coupled to electron transfer. *Proc Natl Acad Sci U S A* **105**: 6803-8
37. Stroud DA, Maher MJ, Lindau C, Vogtle FN, Frazier AE, Surgenor E, Mountford H, Singh AP, Bonas M, Oeljeklaus S*, et al.* (2015) COA6 is a mitochondrial complex IV assembly factor critical for biogenesis of mtDNA-encoded COX2. *Hum Mol Genet* **24**: 5404-15
38. Leary SC, Cobine PA, Kaufman BA, Guercin GH, Mattman A, Palaty J, Lockitch G, Winge DR, Rustin P, Horvath R*, et al.* (2007) The human cytochrome c oxidase assembly factors SCO1 and SCO2 have regulatory roles in the maintenance of cellular copper homeostasis. *Cell Metab* **5**: 9-20
39. Maghool S, Cooray NDG, Stroud DA, Aragao D, Ryan MT, Maher MJ (2019) Structural and functional characterization of the mitochondrial complex IV assembly factor Coa6. *Life Sci Alliance* **2**
40. Lorenzi I, Oeljeklaus S, Aich A, Ronsör C, Callegari S, Dudek J, Warscheid B, Dennerlein S, Rehling P (2018) The mitochondrial TMEM177 associates with COX20 during COX2 biogenesis. *Biochim Biophys Acta Mol Cell Res* **1865**: 323-333
41. Leary SC, Kaufman BA, Pellecchia G, Guercin G-H, Mattman A, Jaksch M, Shoubridge EA (2004) Human SCO1 and SCO2 have independent, cooperative functions in copper delivery to cytochrome c oxidase. *Human Molecular Genetics* **13**: 1839-1848
42. Williams SL, Valnot I, Rustin P, Taanman JW (2004) Cytochrome c oxidase subassemblies in fibroblast cultures from patients carrying mutations in COX10, SCO1, or SURF1. *J Biol Chem* **279**: 7462-9
43. Kovářová N, Pecina P, Nůsková H, Vrbacký M, Zeviani M, Mráček T, Viscomi C, Houštěk J (2016) Tissue- and species-specific differences in cytochrome c oxidase assembly induced by SURF1 defects. *Biochimica et Biophysica Acta (BBA) - Molecular Basis of Disease* **1862**: 705-715
44. Lobo-Jarne T, Perez-Perez R, Fontanesi F, Timon-Gomez A, Wittig I, Penas A, Serrano-Lorenzo P, Garcia-Consuegra I, Arenas J, Martin MA*, et al.* (2020) Multiple pathways coordinate assembly of human mitochondrial complex IV and stabilization of respiratory supercomplexes. *EMBO J* **39**: e103912
45. Perez-Perez R, Lobo-Jarne T, Milenkovic D, Mourier A, Bratic A, Garcia-Bartolome A, Fernandez-Vizarra E, Cadenas S, Delmiro A, Garcia-Consuegra I*, et al.* (2016) COX7A2L Is a Mitochondrial Complex III Binding Protein that Stabilizes the III2+IV Supercomplex without Affecting Respirasome Formation. *Cell Rep* **16**: 2387-98
46. Mick DU, Vukotic M, Piechura H, Meyer HE, Warscheid B, Deckers M, Rehling P (2010) Coa3 and Cox14 are essential for negative feedback regulation of COX1 translation in mitochondria. *J Cell Biol* **191**: 141-54
47. Bourens M, Boulet A, Leary SC, Barrientos A (2014) Human COX20 cooperates with SCO1 and SCO2 to mature COX2 and promote the assembly of cytochrome c oxidase. *Hum Mol Genet* **23**: 2901-13
48. Aich A, Wang C, Chowdhury A, Ronsor C, Pacheu-Grau D, Richter-Dennerlein R, Dennerlein S, Rehling P (2018) COX16 promotes COX2 metallation and assembly during respiratory complex IV biogenesis. *Elife* **7**
49. Bourens M, Barrientos A (2017) A CMC1-knockout reveals translation-independent control of human mitochondrial complex IV biogenesis. *EMBO reports* **18**: 477-494
50. Clemente P, Peralta S, Cruz-Bermudez A, Echevarría L, Fontanesi F, Barrientos A, Fernandez-Moreno MA, Garesse R (2013) hCOA3 stabilizes cytochrome c oxidase 1 (COX1) and promotes cytochrome c oxidase assembly in human mitochondria. *J Biol Chem* **288**: 8321-8331
51. Huigsloot M, Nijtmans LG, Szklarczyk R, Baars MJ, van den Brand MA, Hendriksfranssen MG, van den Heuvel LP, Smeitink JA, Huynen MA, Rodenburg RJ (2011) A mutation in C2orf64 causes

impaired cytochrome c oxidase assembly and mitochondrial cardiomyopathy. *American journal of human genetics* **88**: 488-93

52. Antonicka H, Mattman A, Carlson CG, Glerum DM, Hoffbuhr KC, Leary SC, Kennaway NG, Shoubridge EA (2003) Mutations in COX15 produce a defect in the mitochondrial heme biosynthetic pathway, causing early-onset fatal hypertrophic cardiomyopathy. *American journal of human genetics* **72**: 101-14

53. Dennerlein S, Oeljeklaus S, Jans D, Hellwig C, Bareth B, Jakobs S, Deckers M, Warscheid B, Rehling P (2015) MITRAC7 Acts as a COX1-Specific Chaperone and Reveals a Checkpoint during Cytochrome c Oxidase Assembly. *Cell Reports* **12**: 1644-1655

54. Inoue M, Uchino S, Iida A, Noguchi S, Hayashi S, Takahashi T, Fujii K, Komaki H, Takeshita E, Nonaka I*, et al.* (2019) COX6A2 variants cause a muscle-specific cytochrome c oxidase deficiency. *Annals of neurology* **86**: 193-202

55. Arnaudo E, Hirano M, Sedan RS, Milatovich A, Hsieh C-L, Fabrizi GM, Grossman LI, Francke U, Schon EA (1992) Tissue-specific expression and chromosome assignment of genes specifying two isoforms of subunit VIIa of human cytochrome c oxidase. *Gene* **119**: 299-305

56. Hüttemann M, Schmidt TR, Grossman LI (2003) A third isoform of cytochrome c oxidase subunit VIII is present in mammals. *Gene* **312**: 95-102

57. Fukuda R, Zhang H, Kim JW, Shimoda L, Dang CV, Semenza GL (2007) HIF-1 regulates cytochrome oxidase subunits to optimize efficiency of respiration in hypoxic cells. *Cell* **129**: 111-22

58. Ran FA, Hsu PD, Wright J, Agarwala V, Scott DA, Zhang F (2013) Genome engineering using the CRISPR-Cas9 system. *Nature Protocols* **8**: 2281-2308

59. Schägger H, von Jagow G (1987) Tricine-sodium dodecyl sulfate-polyacrylamide gel electrophoresis for the separation of proteins in the range from 1 to 100 kDa. *Analytical biochemistry* **166**: 368-79

60. Kulak NA, Pichler G, Paron I, Nagaraj N, Mann M (2014) Minimal, encapsulated proteomic-sample processing applied to copy-number estimation in eukaryotic cells. *Nature Methods* **11**: 319-324

61. Giese H, Meisterknecht J, Heidler J, Wittig I (2021) Mitochondrial Complexome Profiling. *Methods in molecular biology (Clifton, NJ)* **2192**: 269-285

62. Brose J, La Fontaine S, Wedd AG, Xiao Z (2014) Redox sulfur chemistry of the copper chaperone Atox1 is regulated by the enzyme glutaredoxin 1, the reduction potential of the glutathione couple GSSG/2GSH and the availability of Cu(I). *Metallomics* **6**: 793-808

63. Rath S, Sharma R, Gupta R, Ast T, Chan C, Durham TJ, Goodman RP, Grabarek Z, Haas ME, Hung WHW*, et al.* (2021) MitoCarta3.0: an updated mitochondrial proteome now with sub-organelle localization and pathway annotations. *Nucleic acids research* **49**: D1541-d1547

64. Stroud DA, Maher MJ, Lindau C, Vögtle FN, Frazier AE, Surgenor E, Mountford H, Singh AP, Bonas M, Oeljeklaus S*, et al.* (2015) Supplemental Table S1 (https://doi.org/10.1093/hmg/ddv265). **[DATASET]**

65. Hock DH, Reljic B, Ang CS, Muellner-Wong L, Mountford HS, Compton AG, Ryan MT, Thorburn DR, Stroud DA (2020) ProteomeXchange, PRIDE PXD016864; Supplemental Table S2 (https://doi.org/10.1074%2Fmcp.RA120.002076). **[DATASET]**

Figure Legends

Figure 1. hTim8a, hTim8b and hTim13 interact together and with Complex IV and intermembrane space proteins.

(A-B) Mitochondria isolated from **(A)** hTim8a$^{KO\ HEK}$ cells with and without hTim8a^{FLAG} re-expression, or **(B)** hTim8b$^{KO\ HEK}$ cells with and without hTim8b^{FLAG} re-expression were compared to mitochondria isolated from control HEK293 cells by SDS-PAGE and immunoblot. Protein expression of the hTim8 protein was induced with tetracycline (Tet) for the indicated time. Representative of n=2 biological replicates.

(C-G) Affinity enrichment mass spectrometry. Mitochondria isolated from **(C)** hTim8a$^{KO\ HEK}$ cells expressing hTim8a^{FLAG}, **(D)** hTim8b$^{KO\ HEK}$ cells expressing hTim8b^{FLAG}, **(E)** hTim8a$^{MUT\ SH}$ cells expressing hTim8a^{FLAG}, **(F)** hTim8b$^{KO\ SH}$ cells expressing hTim8b^{FLAG} and **(G)** wild-type HEK293 cells expressing hTim13^{FLAG} were treated with DSP crosslinker prior to immunoprecipitation with anti-FLAG resin. The $\log_2$ fold change in mean LFQ intensity is plotted against Student's t-test p-value (n=3 biological replicates). Curve indicates significantly enriched proteins. FDR<0.01; **(C)** s0=5.5, **(D)** s0=4.5, **(E)** s0=2, **(F)** s0=5, **(G)** s0=2.5. Functional annotations manually curated.

(H) Sub-mitochondrial localisation of protein interacting partners identified in **(C-G)** compared to the sub-mitochondrial proteome as annotated by the MitoCarta3.0 database [63]. The total uniquely identified proteins (FDR<0.01; orange) and those commonly identified (fold-change >4 in ≥3 of 5 experiments; red). The number of interactors in each mitochondrial compartment indicated as total identified and percentage of total annotated mitochondrial proteins (grey). OM = outer membrane, IMS = intermembrane space, IM = inner membrane, unknown = no localisation annotation.

Data information: **(C-G)** Data presented as $\log_2$(ratio of mean LFQ intensity). Significance determined by unpaired Student's t-test with permutation-based false-discovery rate (FDR) statistics to adjust for multiple hypothesis testing.

Figure 2. Complex IV components and substrates of the MIA import complex are common interactors of hTim8a, hTim8b and hTim13.

(A) 72 proteins were enriched >4-fold in ≥3 of the 5 immunoprecipitation experiments of hTim8a^{FLAG}, hTim8b^{FLAG} and hTim13^{FLAG} in HEK293 and SH-SY5Y cells. These common interacting partners were visualised by known interactions using the STRING database. Functional annotations were manually curated by literature review. Nodes with no connections are proteins that did not have any known interactions with ≥0.500 confidence scoring, as determined by STRING. Dashed border around nodes indicates substrates of the MIA import complex.

(B-C) Changes in protein abundance of hTim8a and hTim8b interactors in mitochondria isolated from **(B)** hTim8a$^{KO\ HEK}$ and hTim8b$^{KO\ HEK}$, or **(C)** hTim8a$^{MUT\ SH}$ and hTim8b$^{KO\ SH}$ cells; determined by quantitative mass spectrometry as published in [15]. Quadrants are labelled with 8a/8b ↑ or ↓ to indicate the increase or decrease of protein abundances in each knock-out cell line. The $\log_2$ fold change in mean LFQ intensity between knock-out and control cells is plotted on each axis. Lines indicate fold change in abundance of ±1.5. n=3 biological replicates for each cell line.

Data information: **(B-C)** Data presented as $\log_2$(ratio of mean LFQ intensity).

Figure 3. COX17 knock-out cells have a COX2 module defect similar to, but more severe than, hTim8-deficient cells.

(A) Changes in protein abundance of Complex IV subunits and assembly factors in mitochondria isolated from hTim8a$^{KO\ HEK}$, hTim8a$^{MUT\ SH}$, hTim8b$^{KO\ HEK}$ and hTim8b$^{KO\ SH}$ cells; by quantitative mass spectrometry published in [15]. The $\log_2$ fold change in mean LFQ intensity between knock-out and control HEK293 and SH-SY5Y cells is shown. '–' indicates protein was undetected. n=3 biological replicates for each cell line. Complex IV proteins listed by module. Transc./Transl. = proteins involved in transcription or translation of Complex IV

genes, SC = subunits involved in supercomplex formation, Aux. or unknown = proteins with auxiliary or unknown functions in Complex IV assembly.

(B-C) Mitochondria isolated from **(B)** $COX17^{MUT\ HEK}$ and **(C)** $COX17^{KO\ SH}$ cells were analysed by quantitative mitochondrial proteomics relative to control cells. The log_2 fold change in mean LFQ intensity is plotted against Student's t-test p-value (n=3 biological replicates). Curve indicates significantly altered proteins; FDR<0.05; s0=0.5. Functional annotations manually curated.

(D) Mitochondria isolated from control cells, $COX17^{MUT\ HEK}$ and $COX17^{KO\ SH}$ cells were analysed by BN-PAGE and immunoblotting with the indicated antibodies. COX4I1-containing complexes indicated as SC: Respiratory supercomplex, $CIII_2$+CIV: Complex III_2-Complex IV complex, CIV_2: Complex IV dimer, CIV: mature Complex IV, and S2*: COX4I1-containing S2 subcomplex. Representative of n=2 biological replicates.

(E) Mitochondria isolated from $COX17^{MUT\ HEK}$ cells complemented with ^{FLAG}COX17 were treated with DSP crosslinker prior to immunoprecipitation with anti-FLAG resin. The log_2 fold change in mean LFQ intensity is plotted against Student's t-test p-value (n=3 biological replicates). Curve indicates significantly enriched proteins; FDR<0.05; s0=7. Functional annotations manually curated.

(F) Intact cells or mitochondria isolated from $hTim8b^{KO\ HEK}$ and control HEK293 cells were subject to ICP-MS analysis to measure copper (Cu) and iron (Fe) content. Abundance is shown as mean ±S.D for metal content per gram of protein. Significance determined by Student's t-test (n=3 biological replicates). **, p<0.01; 'ns' indicates not significant, p>0.05.

(G) Recombinant COA6, hTim8a and hTim8b were purified and incubated, in increasing concentrations, with Cu(I) and bathocuproine disulfonic acid (BCS). Protein-Cu(I) binding outcompetes BCS_2-Cu(I) binding and the decrease in BCS_2-Cu(I) is shown by absorbance, particularly at 482 nm. n=1 biological replicates.

Data information: **(A-C, E)** Data presented as log_2(ratio of mean LFQ intensity). Significance determined by unpaired Student's t-test with permutation-based false-discovery rate (FDR)

statistics to adjust for multiple hypothesis testing. **(F)** Data presented as mean ±S.D. Significance determined by unpaired Student's t-test and p-value threshold of $p<0.05$.

Figure 4. hTim8a and hTim8b function in the progression of the S2 to S3 subcomplex via the incorporation of COX2 module

(A) hTim8a$^{KO\ HEK}$, hTim8b$^{KO\ HEK}$ and control HEK293 cells were pulsed with [35S]-Met/Cys for 2 h in the presence of anisomycin and chased for the indicated times. Isolated mitochondria were analysed by SDS-PAGE, auto-radiography and immunoblot. n=1 biological replicates.

(B-C) [^{35}S]-COX6C and [^{35}S]-COX7C were incubated with mitochondria isolated from **(B)** hTim8a$^{MUT\ SH}$ or **(C)** hTim8b$^{KO\ HEK}$ and control SH-SY5Y or HEK23 cells. Import proceeded in the presence or absence of mitochondrial membrane potential (ΔΨ) for the indicated times. Samples were analysed by BN-PAGE and autoradiography. CBB = Coomassie brilliant blue staining. Representative of n=2 biological replicates.

(D) Constitutive COX4I1^{FLAG} expression was induced in COX17$^{MUT\ HEK}$, hTim8b$^{KO\ HEK}$ and hTim8a$^{MUT\ SH}$ cells in addition to wild-type HEK293 and SH-SY5Y cells. Mitochondria isolated from these cell lines were solubilised in 1% digitonin buffer prior to immunoprecipitation with anti-FLAG resin. The $\log_2$ fold change in mean LFQ intensity (enrichment in knock-out cells compared to wild-type background) is shown. Significance was determined by Student's t-test p-value (n=3 biological replicates) and '+' indicates proteins enriched significantly differently by COX4I1^{FLAG} in the knock-out or wild-type background; FDR<0.05; s0=0.1.

(E) Mitochondria isolated from hTim8a$^{KO\ HEK}$, hTim8b$^{KO\ HEK}$ and control HEK293 cells were resuspended in sodium carbonate solution (pH 9) and centrifuged at 100,000 *g.* Supernatant (Sup) and pellet fractions were analysed by mass spectrometry and normalised against protein abundance in a total fraction (collected prior to centrifugation). The $\log_2$ fold change in normalised mean LFQ intensities between knock-out and control HEK293 cells is shown for subunits of Complex IV (n=3 biological replicates). '–' indicates protein was undetected.

(F) Mitochondria isolated from control, hTim8a$^{MUT\ SH}$ and hTim8b$^{KO\ HEK}$ cells were analysed by BN-PAGE and immunoblotting. COX4I1-containing complexes indicated as SC: Respiratory supercomplex, $CIII_2$+CIV: Complex III_2-Complex IV complex, CIV_2: Complex IV dimer, CIV: mature Complex IV, and S2*: COX4I1-containing S2 subcomplex. Levels of COX4I1 present in subcomplex (*) was quantified as mean ±S.D percentage of COX4I1 present in mature Complex IV (CIV) for each cell line. Significance determined by Student's t-test (hTim8b$^{KO\ HEK}$ n=6 biological replicates; hTim8a$^{MUT\ SH}$ n=4 biological replicates). *, $p<0.05$; **, $p<0.01$.

(G) Mitochondria isolated from control HEK293, COX17$^{MUT\ HEK}$, hTim8a$^{KO\ HEK}$, hTim8b$^{KO\ HEK}$ were analysed by BN-PAGE and immunoblotting with the indicated antibodies. Complexes indicated as SC: Respiratory supercomplex, $CIII_2$+CIV: Complex III_2-Complex IV complex, CIV_2: Complex IV dimer, CIV: mature Complex IV, and S2*: COX4I1-containing S2 subcomplex. Representative of n=2 biological replicates.

Data information: **(D)** Data presented as $\log_2$(ratio of mean LFQ intensity). Significance determined by unpaired Student's t-test with permutation-based false-discovery rate (FDR) statistics to adjust for multiple hypothesis testing. **(E)** Data presented as $\log_2$(ratio of mean LFQ intensity). **(F)** Data presented as mean ±S.D expressed as percentage of the mature Complex IV (CIV) signal.

Figure 5. hTim8a and hTim8b assemble the S3 subcomplex to enable the addition of COX3 module components.

(A) Mitochondria isolated from wild-type HEK293 and hTim8b$^{KO\ HEK}$ SILAC-labelled cells were separated by BN-PAGE. The gel was cut into 60 slices and analysed by LC-MS/MS. Protein abundance was quantified as iBAQ absolute intensity. The relative intensities of Complex IV subunits/assembly factors were hierarchically clustered by Pearson Correlation Distance function. Relative abundances are scaled for each individual protein across both cell lines and all gel slices. Representative BN-PAGE immunoblot is aligned to the complexome profile of control HEK293 cells showing the migration of the S2 subcomplex (left). Enlarged region (red

box) shows proteins only detected in that region and the S2 subcomplex is highlighted (white dashed box). Subunits and assembly factors are coloured by module: Scaffold (green), COX1 (red), COX2 (blue), COX3 (gold). COX4I1-containing complexes by immunoblot indicated as SC: Respiratory supercomplex, $CIII_2$+CIV: Complex III_2-Complex IV complex, CIV: mature Complex IV, and S2*: COX4I1-containing S2 subcomplex. Representative of n=2 biological replicates.

(B-C) Profile plots of iBAQ intensity for Complex IV subunits across the complexome profile of mitochondria isolated from **(B)** hTim8a$^{MUT\ SH}$ and control SH-SY5Y cells; and **(C)** hTim8b$^{KO\ HEK}$ and control HEK293 cells. Subunits are plotted by Complex IV module and iBAQ intensity relative to the maximum intensity of plotted subunits. Solid line indicates subunits from control cells, dashed line from knock-out cells. Complex IV assemblies are indicated as SC: Respiratory supercomplex, $CIII_2$+CIV: Complex III_2-Complex IV complex, CIV: mature Complex IV, and S2*: COX4I1-containing S2 subcomplex. Representative of n=2 biological replicates.

(D) Heatmap showing the changes in the distribution of Complex IV subunits in complexome profiling of mitochondria isolated from hTim8a$^{MUT\ SH}$ (top) and hTim8b$^{KO\ HEK}$ (bottom) compared to controls. Changes in total protein abundance between cell lines were accounted for by normalisation: the abundances of individual proteins (iBAQ intensity) in each slice were expressed as a percentage of their total abundance (as detected across all slices) in the individual cell line (control or knock-out). This treatment, denoting the distribution of Complex IV subunits, indicates the efficiency of assembly. Difference in distribution (% of total protein) was calculated for each slice (KO% - WT%). Negative values indicate a decrease of protein distributed to this region in knock-out cells as an indicator of diminished assembly and vice-versa for positive values. Grey dashed box highlights a region of increased distribution in hTim8a$^{MUT\ SH}$. Complex IV subunits are grouped by module: Scaffold (green), COX1 (red), COX2 (blue), COX3 (gold). Complex IV assemblies are indicated as SC: Respiratory supercomplex, $CIII_2$+CIV: Complex III_2-Complex IV complex, CIV: mature Complex IV, and

S2*: COX4I1-containing S2 subcomplex. Complex III monomer indicated as CIII. Representative of n=2 biological replicates.

(E) Complexome profiling of mitochondria isolated from hTim8a$^{MUT\ SH}$ and control SH-SY5Y cells (top), and hTim8b$^{KO\ HEK}$ and control HEK293 cells (bottom). The relative intensities of Complex IV subunits/assembly factors were hierarchically clustered by Pearson Correlation Distance function. Relative abundances are scaled for each individual protein across both cell lines (knock-out/control) and all gel slices shown. Subunits and assembly factors are coloured by module: Scaffold (green), COX1 (red), COX2 (blue), COX3 (gold). Representative of n=2 biological replicates.

Data information: **(A, E)** Data presented as iBAQ intensity. Normalisation by total iBAQ intensity for each cell line. **(B-C)** Data presented as iBAQ intensity, normalised as in (A) and expressed as a ratio of the maximimum iBAQ intensity. **(D)** Data presented as % of total iBAQ intensity for each protein (Protein A_{slice}/Protein A_{total}). Normalised iBAQ intensities expressed as % of total protein in each cell line and the difference in % (KO-WT) plotted for every gel slice.

Figure 6. hTim8a and hTim8b have distinct functions in Complex IV biogenesis

(A) Mitochondria isolated from hTim8a$^{MUT\ SH}$ cells with and without hTim8b^{FLAG} expression compared to mitochondria from control SH-SY5Y cells were analysed by SDS-PAGE and immunoblotting. Amount of protein after 12 h induction (lanes 4 and 10) was quantified as mean ±S.D percentage of control SH-SY5Y mitochondria. Significance determined by Student's t-test (n=3 biological replicates). *, p<0.05; **, p<0.01; ***, p<0.001; ****,p<0.0001; 'ns' indicates not significant, p>0.05.

(B) Changes in protein abundance in mitochondria isolated from hTim8a$^{MUT\ SH}$ cells with and without hTim8b^{FLAG} expression was quantified using mass spectrometry. The log_2 fold change in mean LFQ intensity (n=3 biological replicates) between knock-out and control SH-SY5Y

cells is shown for the subunits and assembly factors of Complex IV altered in hTim8a$^{MUT\ SH}$ as identified in this analysis and previous mitochondrial proteomics (Fig 3A).

(C) Mitochondria isolated from hTim8a$^{MUT\ SH}$ cells with and without hTim8b^{FLAG} expression compared to mitochondria isolated from control SH-SY5Y cells analysed by BN-PAGE and immunoblotting. COX4I1-containing complexes are indicated as SC: Respiratory supercomplex, $CIII_2$+CIV: Complex III_2-Complex IV complex, CIV_2: Complex IV dimer, CIV: mature Complex IV, and S2*: COX4I1-containing S2 subcomplex. Amount of COX4I1 present in mature monomeric Complex IV (CIV) was quantified as mean ±S.D percentage of control SH-SY5Y mitochondria. Significance determined by Student's t-test (n=3 biological replicates). **, $p<0.001$; ***, $p<0.001$; 'ns' indicates not significant, $p>0.05$.

(D) Mitochondria isolated from hTim8b$^{KO\ HEK}$ cells with and without hTim8a^{FLAG} expression compared to mitochondria isolated from control HEK293 cells by BN-PAGE. hTim8a^{FLAG} expression induced by tetracycline for 8 h. Native protein complexes detected by immunoblot. COX4I1-containing complexes by immunoblot indicated as SC: Respiratory supercomplex, $CIII_2$+CIV: Complex III_2-Complex IV complex, CIV_2: Complex IV dimer, CIV: mature Complex IV, and S2*: COX4I1-containing S2 subcomplex. Amount of COX4I1 present in mature monomeric Complex IV (CIV) was quantified as mean ±S.D percentage of control HEK293 mitochondria. Significance determined by Student's t-test (n=3 biological replicates). **, $p<0.01$; 'ns' indicates not significant, $p>0.05$.

(E) Change in protein abundance in mitochondria isolated from hTim8b$^{KO\ HEK}$ cells with and without hTim8a^{FLAG} expression, by mass-spectrometry. The $\log_2$ fold change in mean LFQ intensity (n=3 biological replicates) between knock-out and control HEK293 cells is shown for subunits and assembly factors of Complex IV altered in hTim8b$^{KO\ HEK}$ as identified in this analysis and previous mitochondrial proteomics (Fig 3A).

Data information: **(A, C-D)** Data presented as mean ±S.D. Significance determined by unpaired Student's t-test and p-value threshold of $p<0.05$. **(B, E)** Data presented as $\log_2$(ratio of mean LFQ intensity).

Tables and their legends

Table 1: Increased abundance of hTim8a, hTim8b and hTim13 correlates with a COX2 defect in $COA6^{KO}$ cells.

STUDY Stroud et al. (2015) Hum. Mol. Genet.#		**CELL LINES** $COA6^{KO}$ HEK293T	
METHOD Isolated mitochondria - SILAC - DDA			
Gene	**Unique peptides**	**Log_2 ($COA6^{KO}$/WT)**	**p-val <0.05†**
TIMM8A	6	1.188	+
TIMM8B	5	0.815	
TIMM13	6	0.989	+
COA6	4	-3.174	+
MT-CO2	7	-4.404	+
COX7A2	3	-1.736	+
NDUFA4	5	-1.585	+
COX6B1	6	-0.920	+
COX6C	4	-0.307	+
COX5B	7	-0.200	+
MT-CO1	2	-0.148	+
COX5A	12	0.126	+
COX4I1	10	0.157	+

Data ref [64]

† p-val = Unpaired Student's t-test p-value

Table 2: Increased abundance of hTim8a, hTim8b and hTim13 correlates with a COX3 defect in HIGD2A^{KO} cells.

STUDY	**CELL LINES**				
Hock et al. (2020) MCP#	HIGD1A^{KO} HEK293T & HIGD2A^{KO} HEK293T				
METHOD					
Isolated mitochondria - TMT - SPS MS3					
Gene	**Unique peptides**	**Log_2 (HIGD1A^{KO}/WT)**	**FDR<5%†**	**Log_2 (HIGD2A^{KO}/WT)**	**FDR<5%†**
TIMM8A	1	-0.280		0.618	
TIMM8B	3	-0.919	+	0.935	+
TIMM13	2	-0.245		0.325	
COX7A2	3	-0.112		-1.490	+
COX6A1	3	-0.118		-1.437	+
NDUFA4	6	-0.113		-1.081	+
COX6B1	5	0.014		-1.075	+
COX7A2L	4	-0.005		-0.137	
COX5A	7	-0.725	+	-0.074	
COX7C	4	-0.349	+	-0.055	
COX6C	4	-0.546	+	-0.030	
COX5B	9	-0.387	+	0.032	
COX4I1	10	-0.691	+	0.035	
COX8A	2	-0.519	+	0.261	

Data ref [65]

† FDR = false-discovery rate. Permutation-based p-value adjustment

Expanded View Figure Legends

Figure EV1. Native affinity enrichment of hTim8b^{FLAG} captures hTim8a and hTim13 but few other interacting partners

(A) Schematic depicting the modular assembly of Complex IV. Complex IV subunits (listed in bold) assemble around core subunits to form modules (COX4I1-COX5A scaffold: green, COX1 module: red, COX2 module: blue, COX3 module: gold) which are progressively combined into subcomplexes. The incorporation of subunits (listed in bold) is enabled by numerous assembly factors (listed in italics).

(B) Mitochondria isolated from hTim8b^{FLAG} expressing cells and control HEK293 cells were solubilised in 1% digitonin buffer prior to immunoprecipitation with anti-FLAG resin. Eluate fractions were processed for mass spectrometry. The $\log_2$ fold change in mean LFQ intensity is plotted against Student's t-test p-value (n=3 biological replicates). Curve indicates significantly enriched proteins; FDR<0.01, s0=4. Functional annotations manually curated.

(C-E) Mitochondria isolated from **(C)** hTim8b$^{KO\ HEK}$ expressing hTim8b^{FLAG}, **(D)** hTim8b$^{KO\ SH}$ expressing hTim8b^{FLAG}, or **(E)** wild-type HEK293 cells expressing hTim10b^{3xFLAG} were treated with DSP crosslinker prior to immunoprecipitation with anti-FLAG resin. The $\log_2$ fold change in mean LFQ intensity is plotted against Student's t-test p-value (n=3 biological replicates). Curve indicates significantly enriched proteins. FDR<0.01, **(C)** s0=7.6, **(D)** s0=2, **(E)** s0=8. Functional annotations were manually curated.

Data information: **(B-E)** Data presented as $\log_2$(ratio of mean LFQ intensity). Significance determined by unpaired Student's t-test with permutation-based false-discovery rate (FDR) statistics to adjust for multiple hypothesis testing.

Figure EV2. hTim8b is not required for the oxidative import of intermembrane space MIA substrates

(A) Mitochondria isolated from wild-type HEK293 cells expressing Mia40^{FLAG} were treated with DSP crosslinker prior to immunoprecipitation with anti-FLAG resin. Eluate fractions were processed for mass spectrometry. The log_2 fold change in mean LFQ intensity is plotted against Student's t-test p-value (n=3 biological replicates). Curve indicates significantly enriched proteins. FDR<0.01, s0=4.5. Functional annotations manually curated.

(B-F) [^{35}S]-Tim23, [^{35}S]-hTim10a, [^{35}S]-COX17, [^{35}S]-COX6B1 and [^{35}S]-COA6 were incubated with mitochondria isolated from hTim8b$^{KO\ HEK}$ or control HEK23 cells for the indicated timepoints. Following import mitochondria were isolated and treated with proteinase K and analysed by SDS-PAGE, autoradiography and immunoblot. The amount of imported [^{35}S]-protein over time was quantified as mean ±S.D and plotted as a percentage of total amount in control mitochondria at 30 min (n=3 biological replicates). 'ns' indicates not significant, p>0.05.

(G) hTim8b$^{KO\ HEK}$ and control HEK293 cells were treated with 5 µM MG132 for 6 h prior to the fractionation of cells into total, mitochondrial (mito), and cytosol fractions by centrifugation. Protein abundance was quantified by LC-MS/MS for MG132, or vehicle (DMSO) treated cells. The log_2 fold change in mean LFQ intensity is shown for known substrates of the MIA import complex (n=3 biological replicates).

(H) Mitochondria isolated from hTim8b$^{KO\ HEK}$ and control HEK293 cells treated with Yme1L siRNA twice over 72 h. Isolated mitochondria were analysed by SDS-PAGE and immunoblot. Representative of n=2 biological replicates.

(I) hTim8b$^{KO\ HEK}$ and control HEK293 cells were treated with Yme1L siRNA twice over 72 h prior to mitochondrial isolation. Protein abundance in isolated mitochondria was quantified by LC-MS/MS for Yme1L-siRNA and scramble-siRNA (control) treated cells. The log_2 fold change in mean LFQ intensity (n=3 biological replicates) is shown for proposed Yme1L substrates [32] and hTim8b^{FLAG} interactors are labelled in bold. '–' indicates protein was undetected.

Data information: **(A)** Data presented as log_2(ratio of mean LFQ intensity). Significance determined by unpaired Student's t-test with permutation-based false-discovery rate (FDR) statistics to adjust for multiple hypothesis testing. **(B-F)** Data presented as mean ±S.D.

Significance determined by unpaired Student's t-test and p-value threshold of $p<0.05$. **(G, I)** Data presented as log_2(ratio of mean LFQ intensity).

Figure EV3. hTim8-deficient cells display a similar, but milder, COX2/COX3 module defect compared to knock-out of COX17.

(A) Topographical heatmap showing protein abundance changes in $hTim8a^{MUT\ SH}$ and $hTim8b^{KO\ SH}$ mitochondria compared to control SH-SY5Y mitochondria. Log_2 fold change in mean LFQ intensity is mapped to the structure of human Complex IV (PDB5Z62).

(B) $hTim8b^{KO\ HEK}$ cells with and without $hTim8b^{FLAG}$, $hTim8a^{KO\ HEK}$ and control HEK293 cells were treated with 10 µM menadione for 2 h. Extracellular H_2O_2 was detected by luciferase-reporter luminescence using ROS-Glo™ H_2O_2 Assay (Promega). Relative luminescence units (RLU) were quantified as mean ±S.D and significance determined by Student's t-test ($hTim8b^{KO}$ n=4 technical replicates, $hTim8a^{KO}$ n=3 technical replicates). *, $p<0.05$; **, $p<0.01$; ***, $p<0.001$; ****, $p<0.0001$; 'ns' indicates not significant, $p>0.05$. $hTim8b^{KO\ HEK}$/$hTim8b^{KO\ HEK}$+$hTim8b^{FLAG}$ analysis representative of n=2 biological replicates. $hTim8a^{KO\ HEK}$ analysis n=1 biological replicates.

(C) Validation of CRISPR/Cas9 gene-editing in $COX17^{MUT\ HEK}$ and $COX17^{KO\ SH}$ cells. Isolated mitochondria from gene-edited cells were compared to control HEK293 or SH-SY5Y cells by SDS-PAGE and immunoblot. CRISPR/Cas9 guide-RNA targeted exon 1 of the *COX17* gene. Mass spectrometric analysis of mitochondria isolated from COX17-deficient cells and control HEK293 or SH-SY5Y cells shows multiple peptides were detected in control cells, but not in CRISPR/Cas9-edited cells.

(D) Topographical heatmap showing protein abundance changes in $COX17^{MUT\ HEK}$ and $COX17^{KO\ SH}$ mitochondria compared to control HEK293 or SH-SY5Y mitochondria. Log_2 fold change in mean LFQ intensity is mapped to the structure of human Complex IV (PDB5Z62).

Data information: **(A, D)** Data presented as log_2(ratio of mean LFQ intensity). **(B)** Data presented as mean ±S.D. Significance determined by unpaired Student's t-test and p-value threshold of $p<0.05$.

Figure EV4. Human Tim8 proteins are each stable in heterohexameric complex with hTim13.

(A-C) Recombinant **(A)** hTim8a and hTim13, **(B)** hTim8b and hTim13, or **(C)** hTim8a and hTim13 were combined and purified prior to separation by size-exclusion chromatography (SEC). The protein content of fractions taken from SEC was quantified by absorbance at 280 nm and normalised as percentage of maximum absorbance. Fractions were analysed by SDS-PAGE and in-gel protein staining. Representative of n=2 biological replicates.

(D) Recombinant hTim8a was incubated with co-purified hTim8b-hTim13 (left) and hTim8b incubated with hTim8a-hTim13 (right) in equimolar concentrations, prior to separation by size-exclusion chromatography (SEC). The protein content of fractions taken from SEC was quantified by absorbance at 280 nm and normalised as percentage of maximum absorbance. Fractions were analysed by SDS-PAGE and in-gel protein staining. n=1 biological replicates.

(E-F) Example intact protein mass spectra. Co-purified recombinant hTim8a-hTim13 complex(es) were analysed by **(E)** native mass spectrum at 200 mM ammonium acetate (pH 7.0), showing the characteristic shifting of the charge envelope to lower charge state at higher m/z (Inset: zoom-in on lowly charged masses at up to 5,000m/z); and, **(F)** denaturing mass spectrum (0.1% formic acid and acetonitrile), showing the highly charged monomers at lower m/z. n=1 biological replicates.

(G) Deconvoluted spectra from the denaturing mass spectra of recombinant hTim8a-hTim13 complex (left) and recombinant hTim8b (right), showing the presence of monomers of hTim8a (11,406 Da), hTim13 (10,906 Da) and hTim8b (9,751 Da). n=1 biological replicates.

(H) Deconvoluted spectra from the native mass spectra of recombinant hTim8a-hTim13 complex (left) and recombinant hTim8b-hTim13 (right), showing the presence of the heterohexameric complexes calculated to be in 3:3 stoichiometry in both cases ($hTim8a_3$-$hTim13_3$ = 66,940 Da; $hTim8b_3$-$hTim13_3$ = 61,976 Da). n=1 biological replicates

Data information: No statistical treatments.

Figure EV5. hTim8a-hTim13 and hTim8b-hTim13 complexes interact in mitochondria

(A) [^{35}S]-hTim13, [^{35}S]-hTim8a and [^{35}S]-hTim8b were incubated with mitochondria isolated from wild-type HEK293 cells for 15 or 60 min. Following import mitochondria were isolated and treated with proteinase K and analysed by BN-PAGE and autoradiography. Representative of n=3 biological replicates.

(B) [^{35}S]-hTim8a was imported into control and mitochondria isolated from cells expressing hTim8b^{FLAG} or hTim13^{FLAG}, **(C)** [^{35}S]-hTim8b was imported into control and mitochondria isolated from cells expressing hTim8a^{FLAG} or hTim13^{FLAG}; and **(D)** [^{35}S]-Tim22 was incubated with control and mitochondria isolated from cells expressing hTim10b^{3xFLAG}. Following import mitochondria were treated with proteinase K and then solubilised in the absence or presence of the indicated antibodies. Interaction in native complexes analysed by BN-PAGE and autoradiography. CBB = coommassie brilliant blue staining. Representative of n=2 biological replicates.

(D) Mitochondria isolated from hTim8b$^{KO\ HEK}$ and hTim8b$^{KO\ SH}$ cells were compared to mitochondria from control HEK293 and SH-SY5Y cells by BN-PAGE analysis and immunoblot. hTim8b$^{KO\ HEK}$ analysis representative of n=3 biological replicates. hTim8b$^{KO\ SH}$ analysis n=1 biological replicates

(E-F) Mitochondria isolated from wild-type HEK293 cells, treated twice over 72 h with hTim13-siRNA, were analysed by **(E)** SDS-PAGE and immunoblot, or **(F)** BN-PAGE and immunoblot. hTim13 levels were quantified as mean ±S.D percentage of cells treated with control siRNA.

Significance determined by Student's t-test (n=3 biological replicates.). *, $p<0.05$. **(E)** Representative of n=3 biological replicates. **(F)** Representative of n=2 biological replicates.

(G) Wild-type HEK293 cells were treated with hTim13 siRNA twice over 72 h prior to mitochondrial isolation. Protein abundance in isolated mitochondria was quantified by LC-MS/MS for hTim13-siRNA and scramble-siRNA (control) treated cells. The $\log_2$ fold change in mean LFQ intensity is plotted against Student's t-test p-value (n=3 biological replicates). Curve indicates significantly altered proteins; FDR<0.05; s0=0.5. Functional annotations manually curated.

Data information: **(E)** Data presented as mean ±S.D. Significance determined by unpaired Student's t-test and p-value threshold of $p<0.05$. **(G)** Data presented as $\log_2$(ratio of mean LFQ intensity). Significance determined by unpaired Student's t-test with permutation-based false-discovery rate (FDR) statistics to adjust for multiple hypothesis testing.

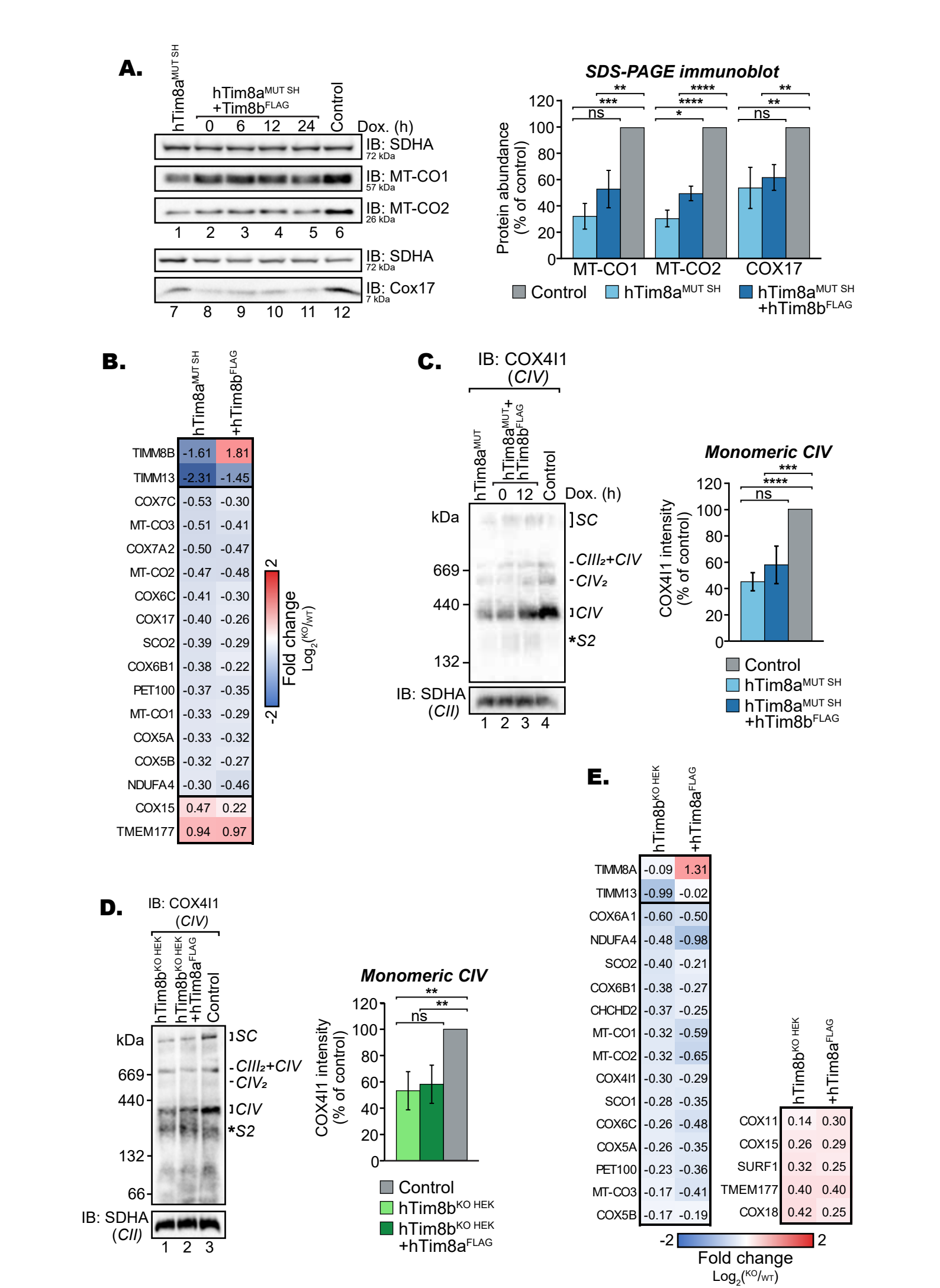

Anderson et al. Figure 6

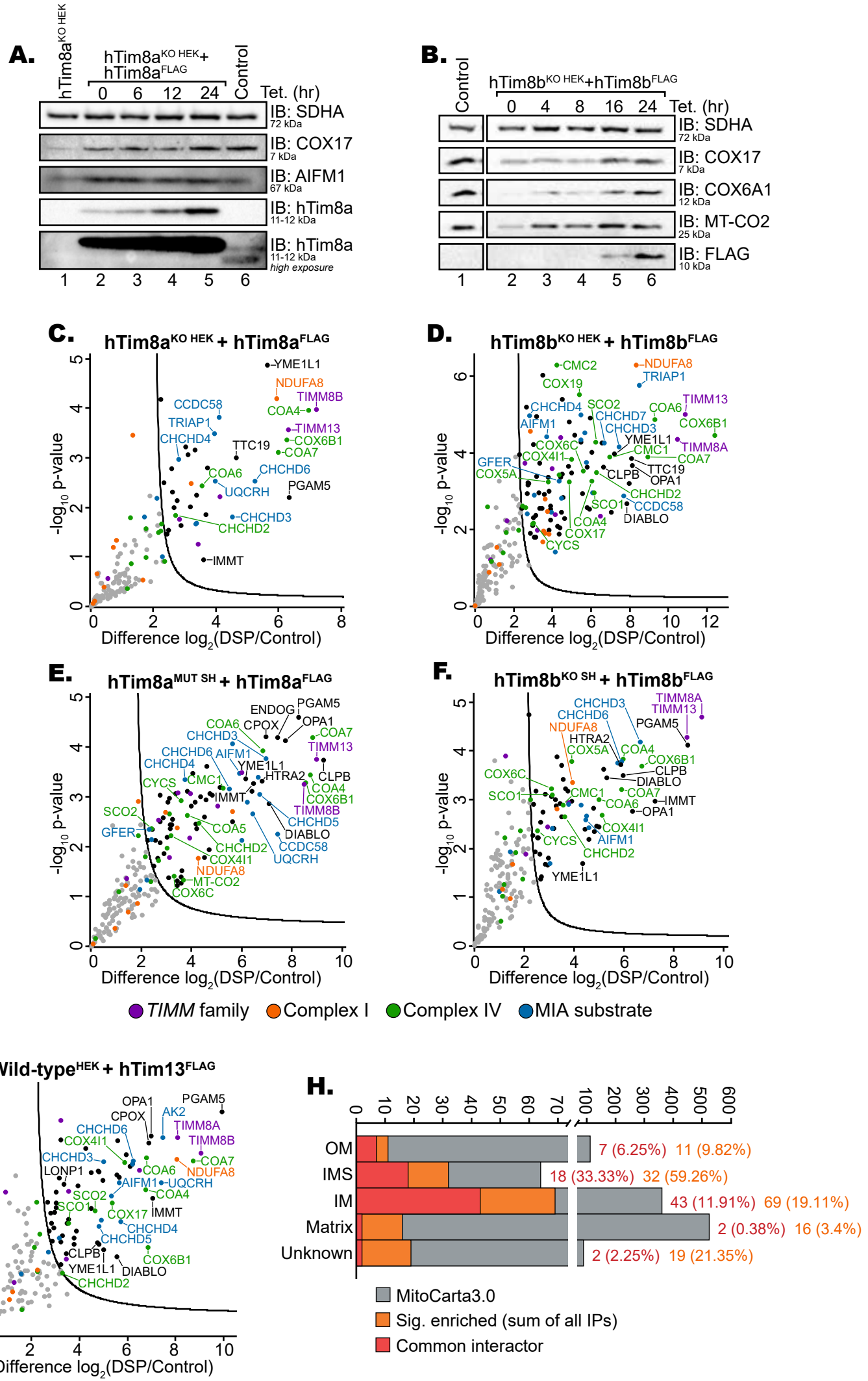

Anderson et al. Figure 1

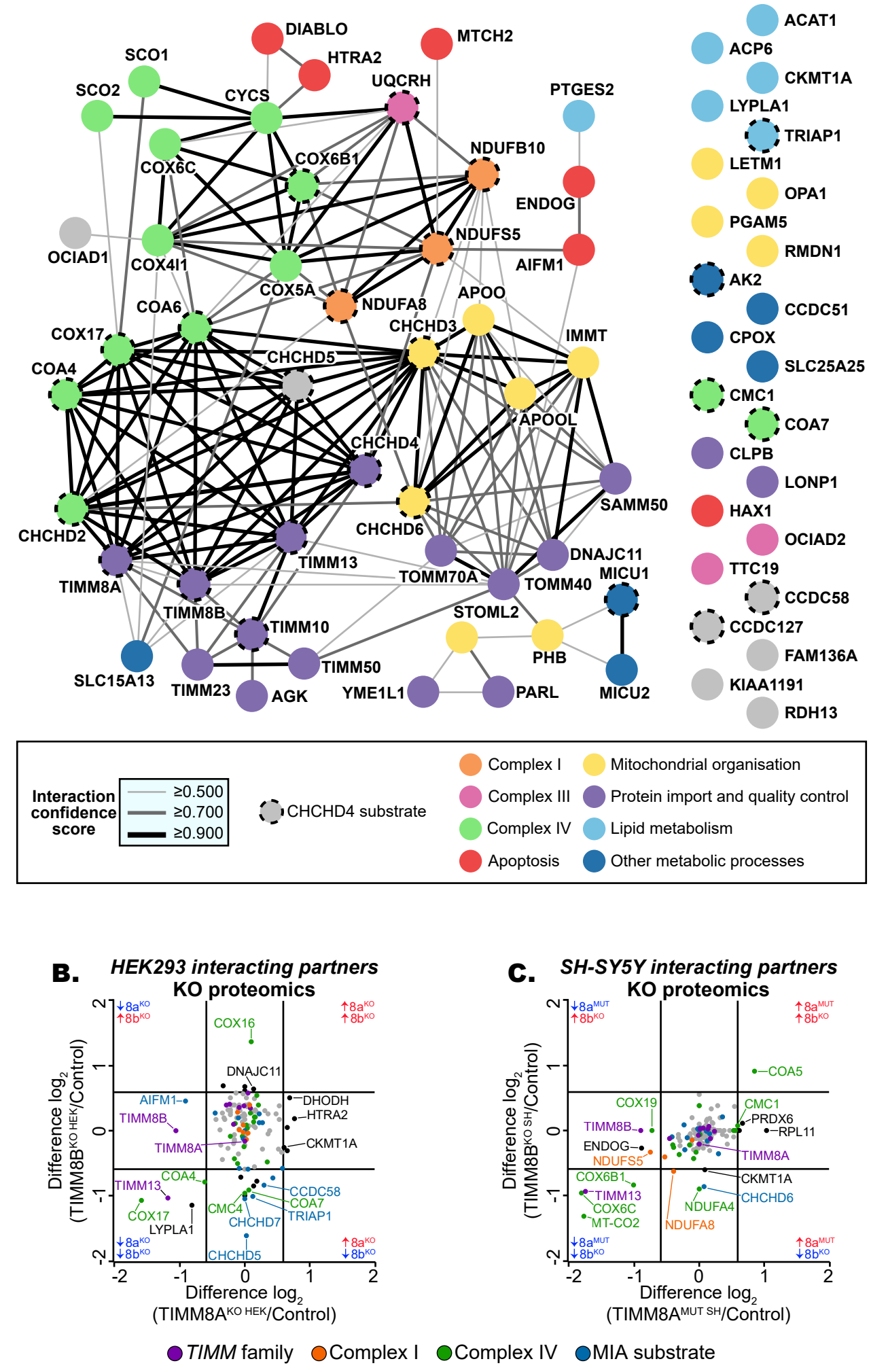

Anderson et al. Figure 2

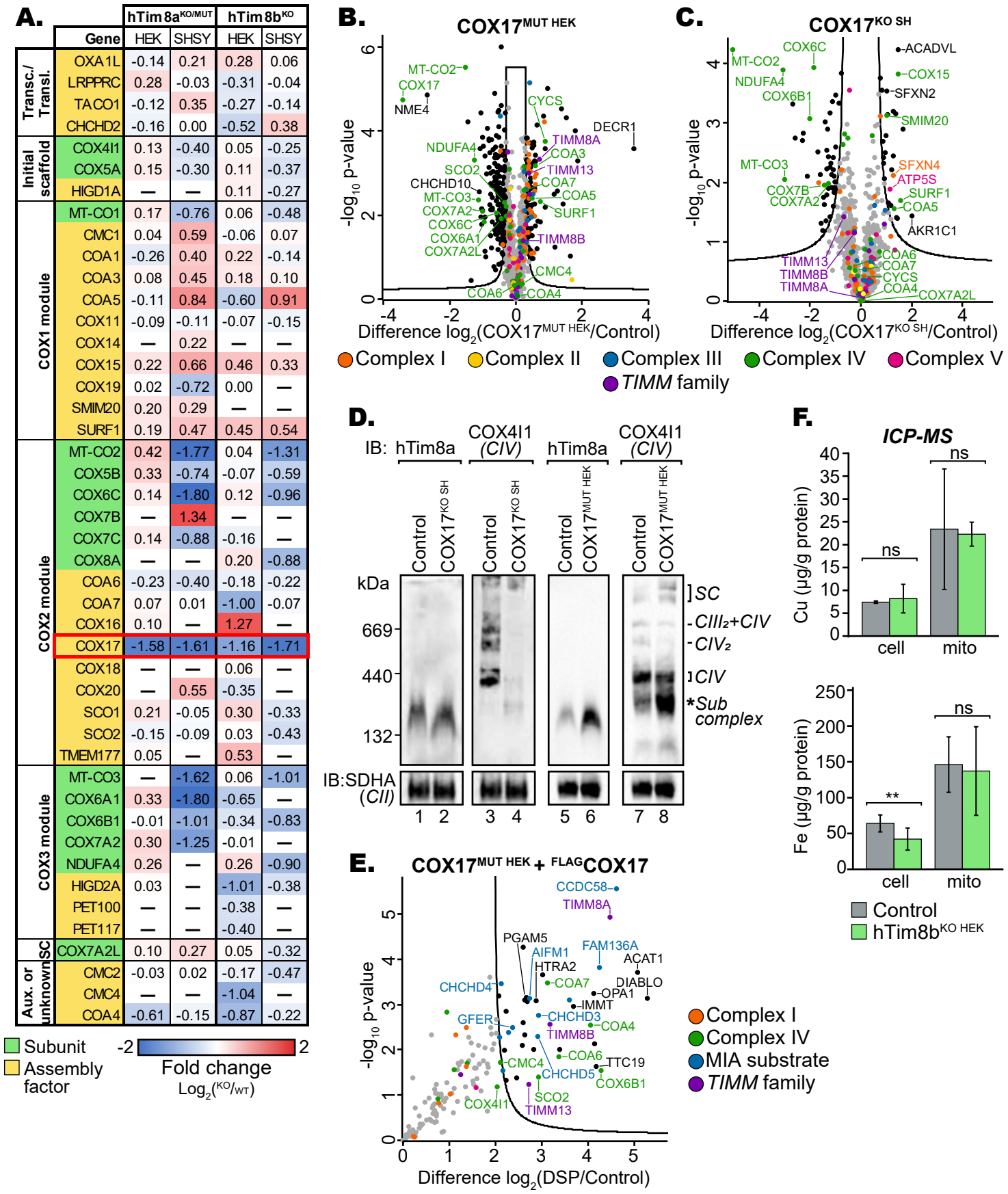

Anderson et al. Figure 3

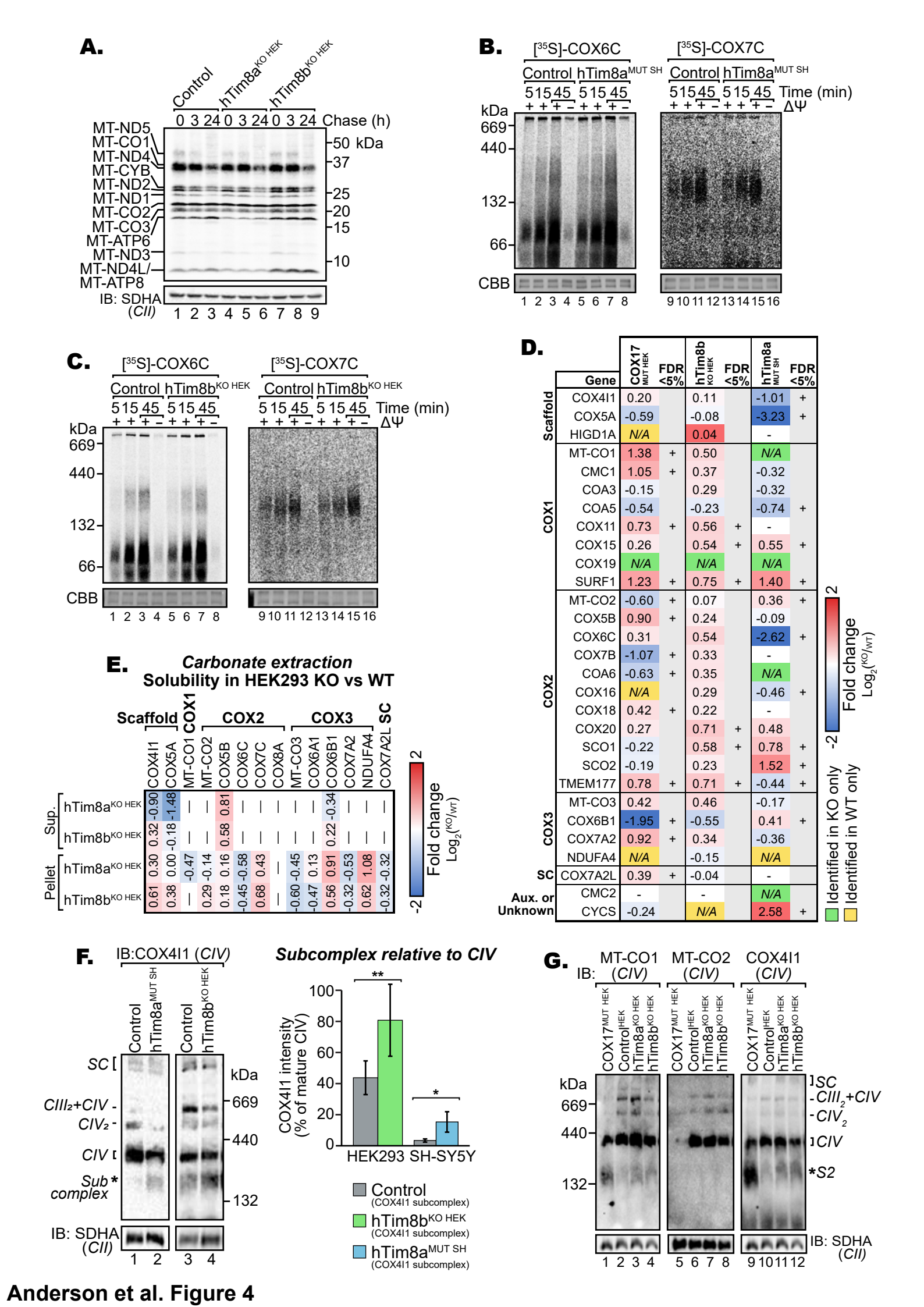

Anderson et al. Figure 4

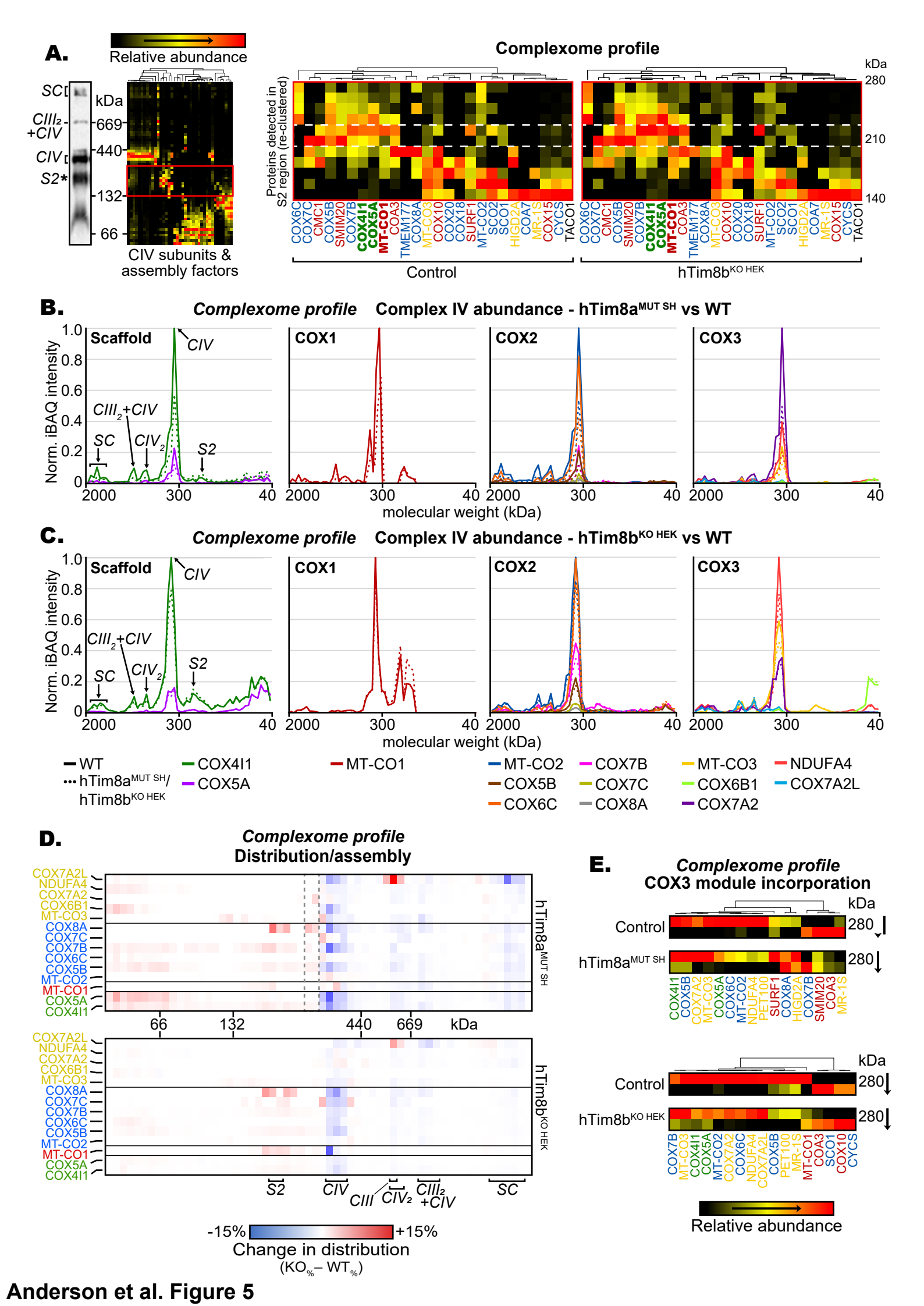

Anderson et al. Figure 5

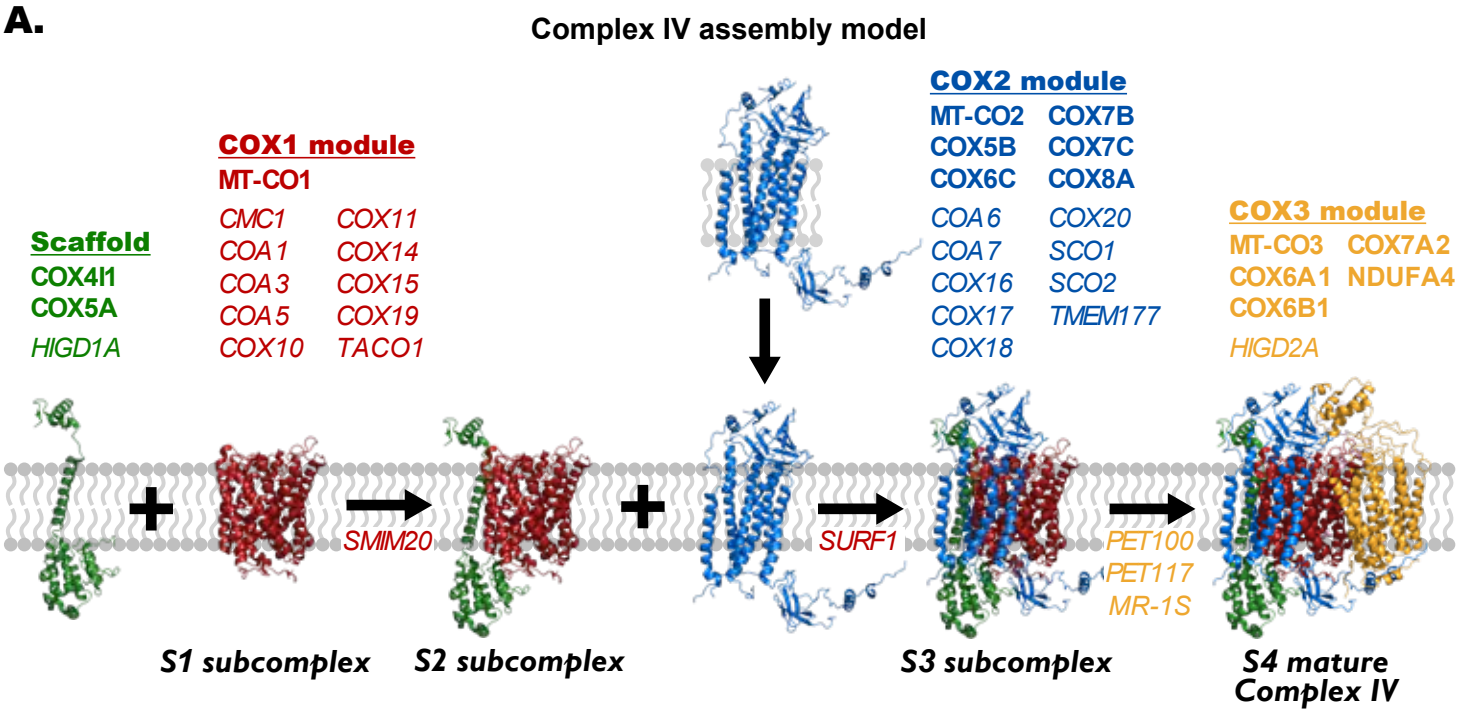

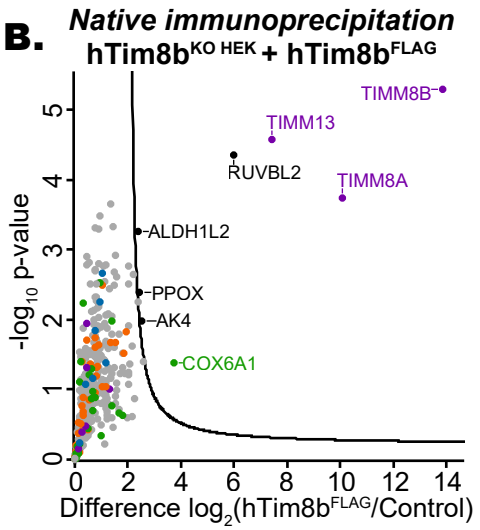

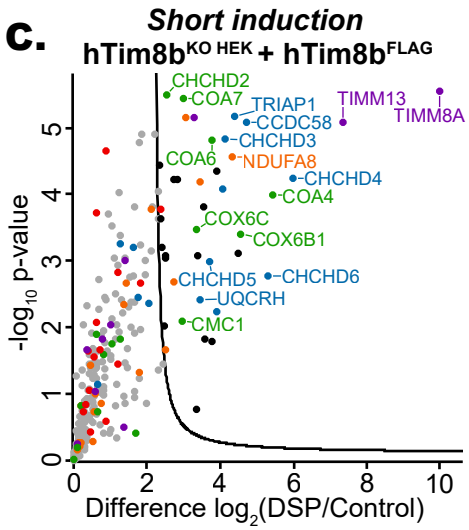

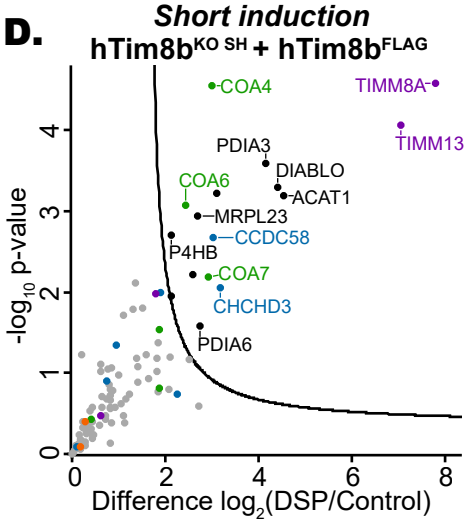

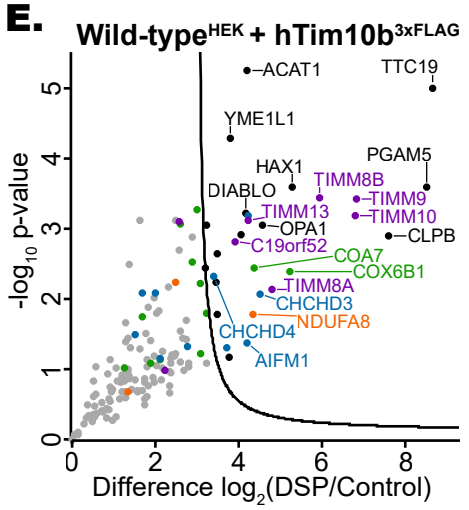

Complex I Complex IV MIA substrate *TIMM* family

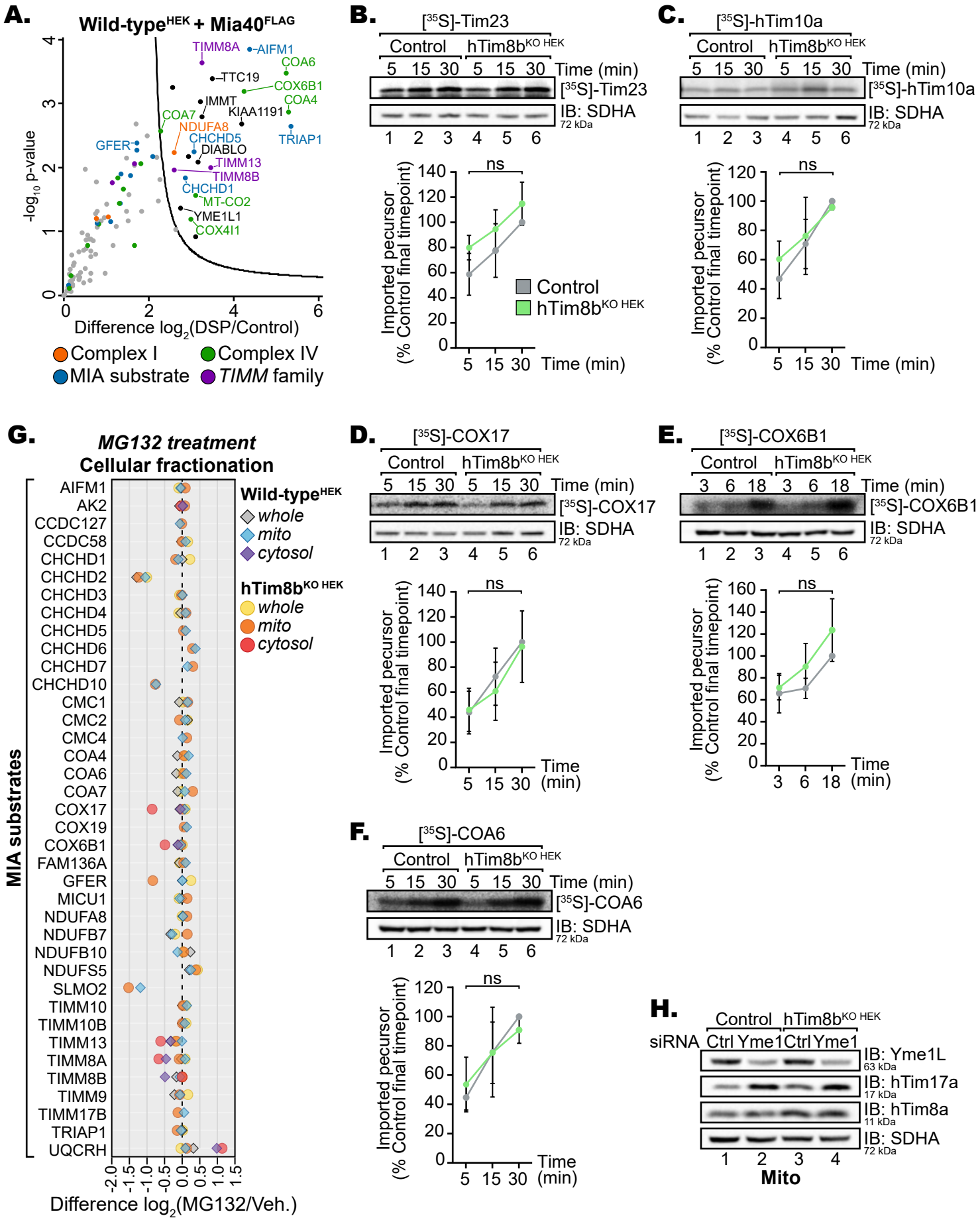

Anderson et al. Expanded View 2

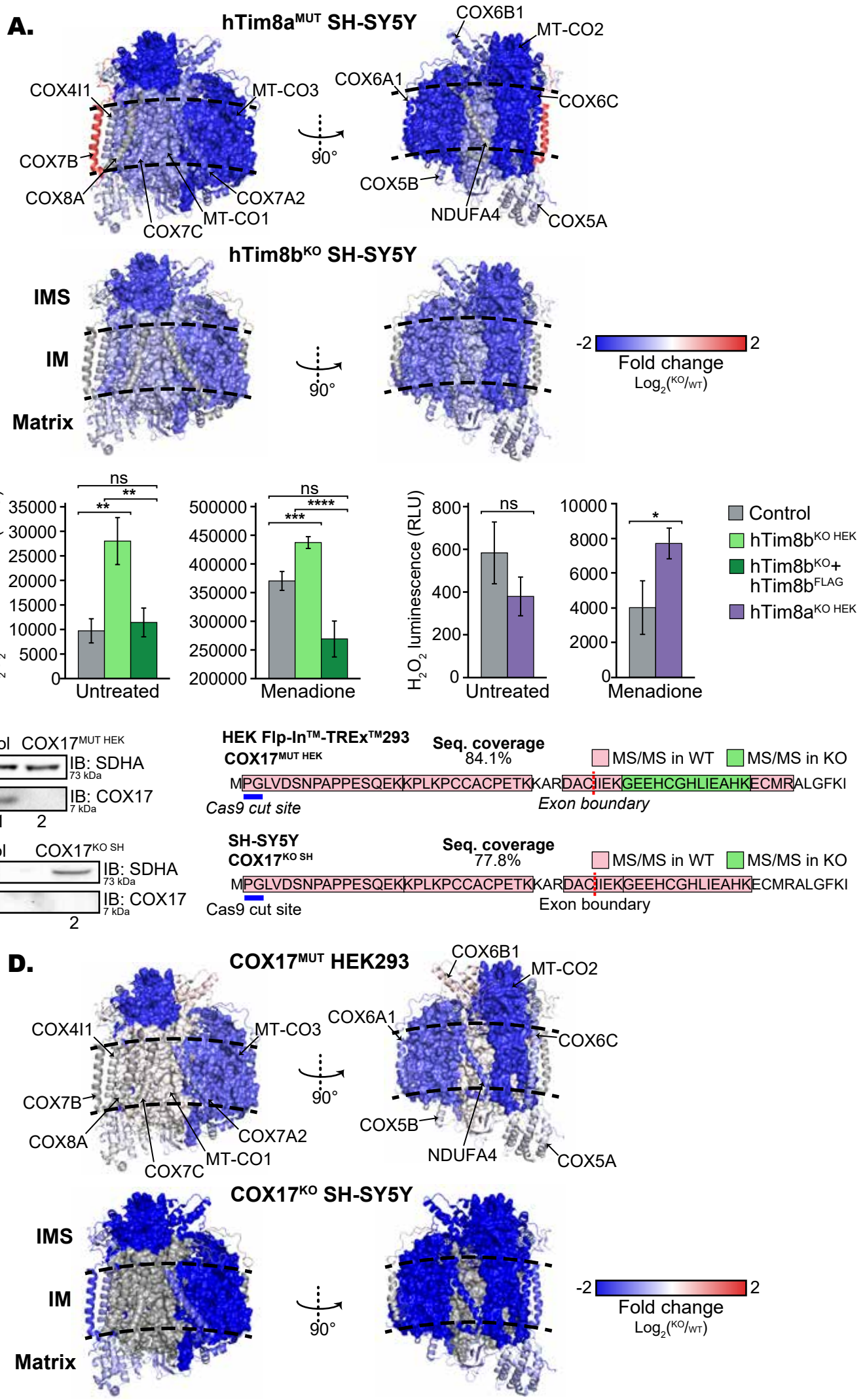

Anderson et al. Expanded View 3

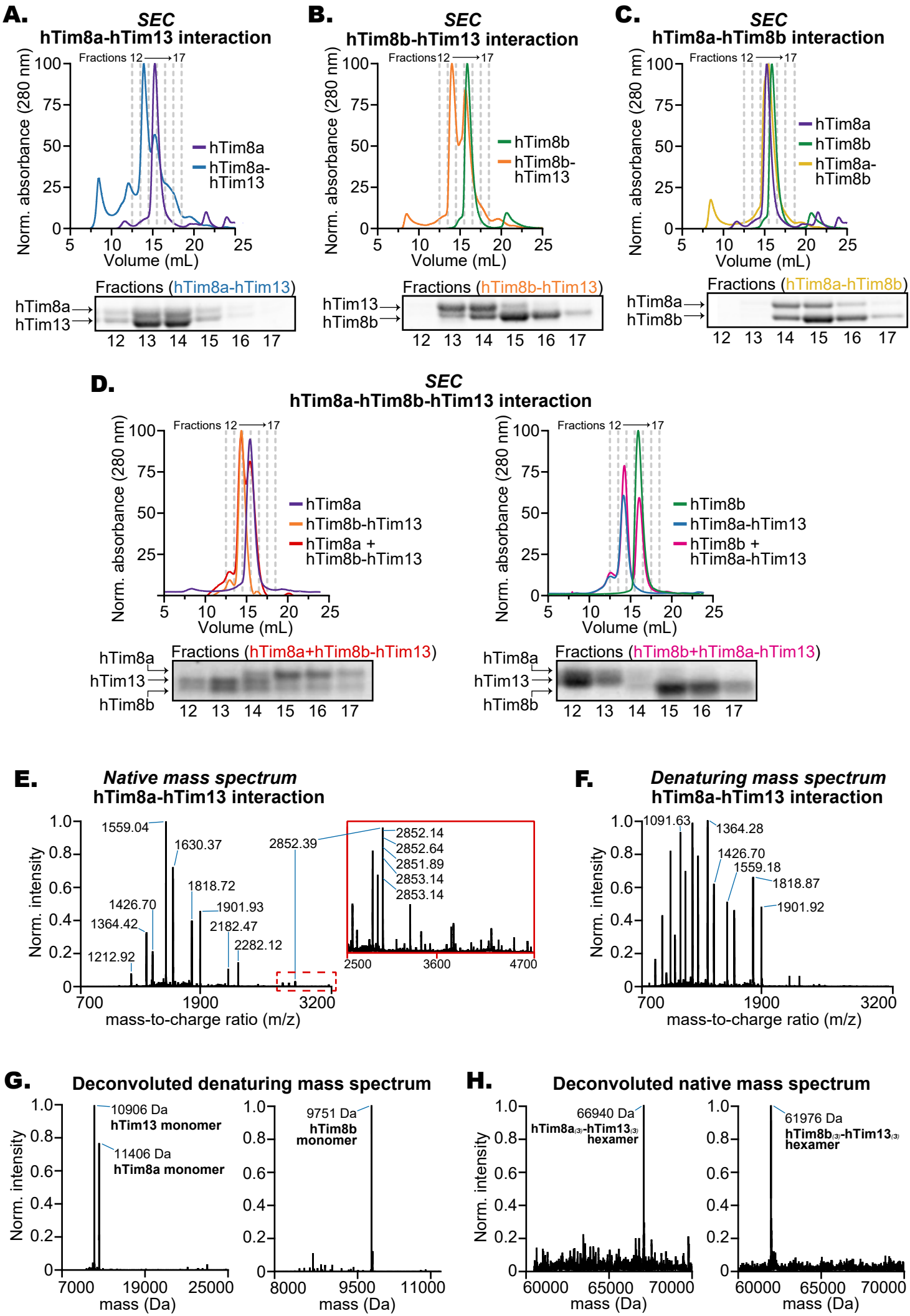

Anderson et al. Expanded View 4

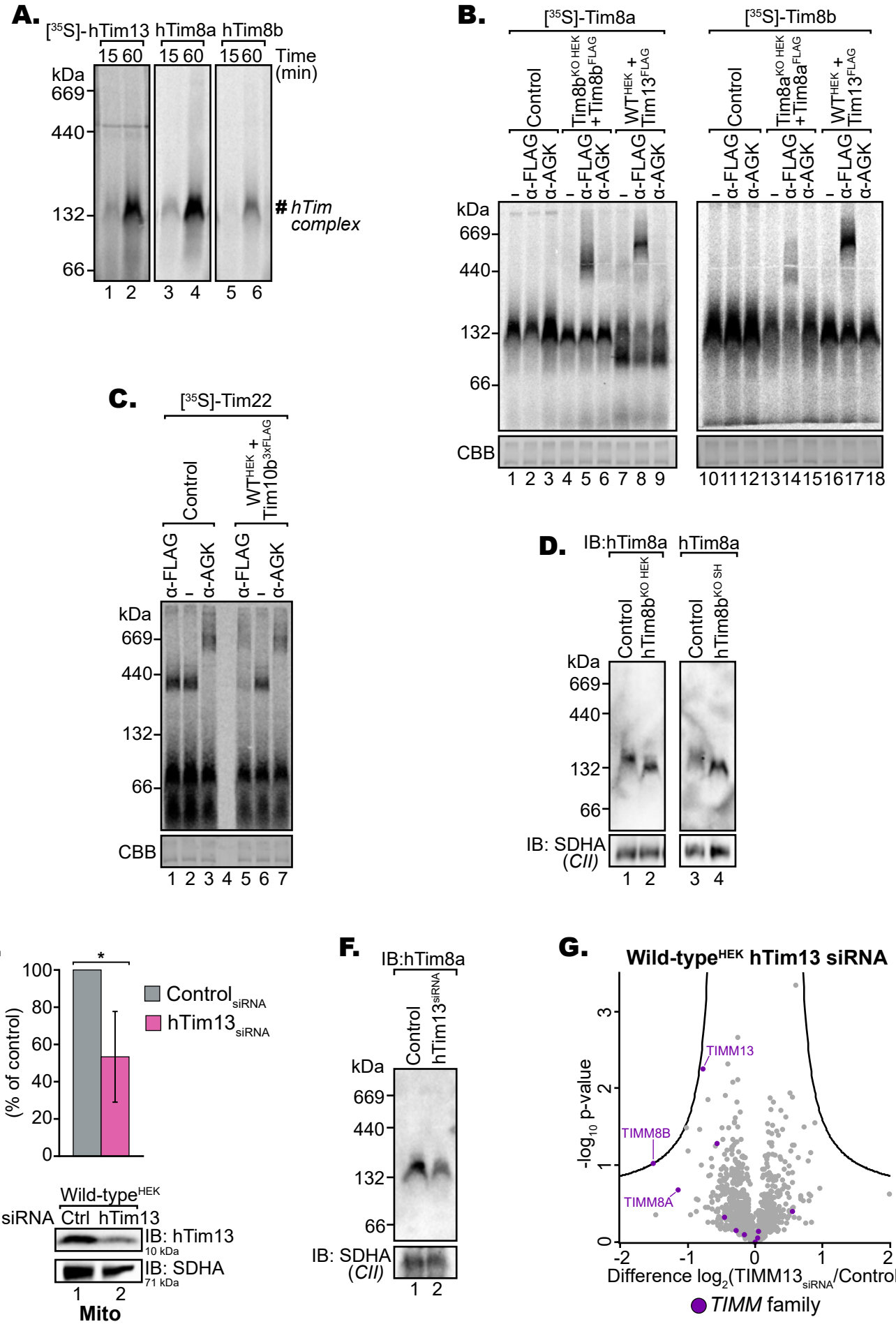

Anderson et al. Expanded View 5